

1

AD-A256 612



AFIT/GE/ENG/92S-03

DTIC
ELECTE
OCT 27 1992
S
C

**THE DETECTION AND CORRELATION
MODELING OF RAYLEIGH DISTRIBUTED
RADAR SIGNALS**

THESIS

Alan Lee Buterbaugh
Captain, USAF

AFIT/GE/ENG/92S-03

Approved for public release; Distribution Unlimited

92-28125



012225

76877

AFIT/GE/ENG/92S-03

THE DETECTION AND CORRELATION
MODELING OF RAYLEIGH DISTRIBUTED
RADAR SIGNALS

THESIS

Presented to the Faculty of the School of Engineering
of the Air Force Institute of Technology
Air University
In Partial Fulfillment of the
Requirements for the Degree of
Master of Science in Electrical Engineering

Alan Lee Buterbaugh, B.S.
Captain, USAF

September, 1992

Approved for public release; Distribution Unlimited

AFIT/GE/ENG/92S-03
1
2
3
4
5
6
7
8
9
10
11
12
13
14
15
16
17
18
19
20
21
22
23
24
25
26
27
28
29
30
31
32
33
34
35
36
37
38
39
40
41
42
43
44
45
46
47
48
49
50
51
52
53
54
55
56
57
58
59
60
61
62
63
64
65
66
67
68
69
70
71
72
73
74
75
76
77
78
79
80
81
82
83
84
85
86
87
88
89
90
91
92
93
94
95
96
97
98
99
100
101
102
103
104
105
106
107
108
109
110
111
112
113
114
115
116
117
118
119
120
121
122
123
124
125
126
127
128
129
130
131
132
133
134
135
136
137
138
139
140
141
142
143
144
145
146
147
148
149
150
151
152
153
154
155
156
157
158
159
160
161
162
163
164
165
166
167
168
169
170
171
172
173
174
175
176
177
178
179
180
181
182
183
184
185
186
187
188
189
190
191
192
193
194
195
196
197
198
199
200
201
202
203
204
205
206
207
208
209
210
211
212
213
214
215
216
217
218
219
220
221
222
223
224
225
226
227
228
229
230
231
232
233
234
235
236
237
238
239
240
241
242
243
244
245
246
247
248
249
250
251
252
253
254
255
256
257
258
259
260
261
262
263
264
265
266
267
268
269
270
271
272
273
274
275
276
277
278
279
280
281
282
283
284
285
286
287
288
289
290
291
292
293
294
295
296
297
298
299
300
301
302
303
304
305
306
307
308
309
310
311
312
313
314
315
316
317
318
319
320
321
322
323
324
325
326
327
328
329
330
331
332
333
334
335
336
337
338
339
340
341
342
343
344
345
346
347
348
349
350
351
352
353
354
355
356
357
358
359
360
361
362
363
364
365
366
367
368
369
370
371
372
373
374
375
376
377
378
379
380
381
382
383
384
385
386
387
388
389
390
391
392
393
394
395
396
397
398
399
400
401
402
403
404
405
406
407
408
409
410
411
412
413
414
415
416
417
418
419
420
421
422
423
424
425
426
427
428
429
430
431
432
433
434
435
436
437
438
439
440
441
442
443
444
445
446
447
448
449
450
451
452
453
454
455
456
457
458
459
460
461
462
463
464
465
466
467
468
469
470
471
472
473
474
475
476
477
478
479
480
481
482
483
484
485
486
487
488
489
490
491
492
493
494
495
496
497
498
499
500
501
502
503
504
505
506
507
508
509
510
511
512
513
514
515
516
517
518
519
520
521
522
523
524
525
526
527
528
529
530
531
532
533
534
535
536
537
538
539
540
541
542
543
544
545
546
547
548
549
550
551
552
553
554
555
556
557
558
559
560
561
562
563
564
565
566
567
568
569
570
571
572
573
574
575
576
577
578
579
580
581
582
583
584
585
586
587
588
589
590
591
592
593
594
595
596
597
598
599
600
601
602
603
604
605
606
607
608
609
610
611
612
613
614
615
616
617
618
619
620
621
622
623
624
625
626
627
628
629
630
631
632
633
634
635
636
637
638
639
640
641
642
643
644
645
646
647
648
649
650
651
652
653
654
655
656
657
658
659
660
661
662
663
664
665
666
667
668
669
670
671
672
673
674
675
676
677
678
679
680
681
682
683
684
685
686
687
688
689
690
691
692
693
694
695
696
697
698
699
700
701
702
703
704
705
706
707
708
709
710
711
712
713
714
715
716
717
718
719
720
721
722
723
724
725
726
727
728
729
730
731
732
733
734
735
736
737
738
739
740
741
742
743
744
745
746
747
748
749
750
751
752
753
754
755
756
757
758
759
760
761
762
763
764
765
766
767
768
769
770
771
772
773
774
775
776
777
778
779
780
781
782
783
784
785
786
787
788
789
790
791
792
793
794
795
796
797
798
799
800
801
802
803
804
805
806
807
808
809
810
811
812
813
814
815
816
817
818
819
820
821
822
823
824
825
826
827
828
829
830
831
832
833
834
835
836
837
838
839
840
841
842
843
844
845
846
847
848
849
850
851
852
853
854
855
856
857
858
859
860
861
862
863
864
865
866
867
868
869
870
871
872
873
874
875
876
877
878
879
880
881
882
883
884
885
886
887
888
889
890
891
892
893
894
895
896
897
898
899
900
901
902
903
904
905
906
907
908
909
910
911
912
913
914
915
916
917
918
919
920
921
922
923
924
925
926
927
928
929
930
931
932
933
934
935
936
937
938
939
940
941
942
943
944
945
946
947
948
949
950
951
952
953
954
955
956
957
958
959
960
961
962
963
964
965
966
967
968
969
970
971
972
973
974
975
976
977
978
979
980
981
982
983
984
985
986
987
988
989
990
991
992
993
994
995
996
997
998
999
1000
1001
1002
1003
1004
1005
1006
1007
1008
1009
1010
1011
1012
1013
1014
1015
1016
1017
1018
1019
1020
1021
1022
1023
1024
1025
1026
1027
1028
1029
1030
1031
1032
1033
1034
1035
1036
1037
1038
1039
1040
1041
1042
1043
1044
1045
1046
1047
1048
1049
1050
1051
1052
1053
1054
1055
1056
1057
1058
1059
1060
1061
1062
1063
1064
1065
1066
1067
1068
1069
1070
1071
1072
1073
1074
1075
1076
1077
1078
1079
1080
1081
1082
1083
1084
1085
1086
1087
1088
1089
1090
1091
1092
1093
1094
1095
1096
1097
1098
1099
1100
1101
1102
1103
1104
1105
1106
1107
1108
1109
1110
1111
1112
1113
1114
1115
1116
1117
1118
1119
1120
1121
1122
1123
1124
1125
1126
1127
1128
1129
1130
1131
1132
1133
1134
1135
1136
1137
1138
1139
1140
1141
1142
1143
1144
1145
1146
1147
1148
1149
1150
1151
1152
1153
1154
1155
1156
1157
1158
1159
1160
1161
1162
1163
1164
1165
1166
1167
1168
1169
1170
1171
1172
1173
1174
1175
1176
1177
1178
1179
1180
1181
1182
1183
1184
1185
1186
1187
1188
1189
1190
1191
1192
1193
1194
1195
1196
1197
1198
1199
1200
1201
1202
1203
1204
1205
1206
1207
1208
1209
1210
1211
1212
1213
1214
1215
1216
1217
1218
1219
1220
1221
1222
1223
1224
1225
1226
1227
1228
1229
1230
1231
1232
1233
1234
1235
1236
1237
1238
1239
1240
1241
1242
1243
1244
1245
1246
1247
1248
1249
1250
1251
1252
1253
1254
1255
1256
1257
1258
1259
1260
1261
1262
1263
1264
1265
1266
1267
1268
1269
1270
1271
1272
1273
1274
1275
1276
1277
1278
1279
1280
1281
1282
1283
1284
1285
1286
1287
1288
1289
1290
1291
1292
1293
1294
1295
1296
1297
1298
1299
1300
1301
1302
1303
1304
1305
1306
1307
1308
1309
1310
1311
1312
1313
1314
1315
1316
1317
1318
1319
1320
1321
1322
1323
1324
1325
1326
1327
1328
1329
1330
1331
1332
1333
1334
1335
1336
1337
1338
1339
1340
1341
1342
1343
1344
1345
1346
1347
1348
1349
1350
1351
1352
1353
1354
1355
1356
1357
1358
1359
1360
1361
1362
1363
1364
1365
1366
1367
1368
1369
1370
1371
1372
1373
1374
1375
1376
1377
1378
1379
1380
1381
1382
1383
1384
1385
1386
1387
1388
1389
1390
1391
1392
1393
1394
1395
1396
1397
1398
1399
1400
1401
1402
1403
1404
1405
1406
1407
1408
1409
1410
1411
1412
1413
1414
1415
1416
1417
1418
1419
1420
1421
1422
1423
1424
1425
1426
1427
1428
1429
1430
1431
1432
1433
1434
1435
1436
1437
1438
1439
1440
1441
1442
1443
1444
1445
1446
1447
1448
1449
1450
1451
1452
1453
1454
1455
1456
1457
1458
1459
1460
1461
1462
1463
1464
1465
1466
1467
1468
1469
1470
1471
1472
1473
1474
1475
1476
1477
1478
1479
1480
1481
1482
1483
1484
1485
1486
1487
1488
1489
1490
1491
1492
1493
1494
1495
1496
1497
1498
1499
1500
1501
1502
1503
1504
1505
1506
1507
1508
1509
1510
1511
1512
1513
1514
1515
1516
1517
1518
1519
1520
1521
1522
1523
1524
1525
1526
1527
1528
1529
1530
1531
1532
1533
1534
1535
1536
1537
1538
1539
1540
1541
1542
1543
1544
1545
1546
1547
1548
1549
1550
1551
1552
1553
1554
1555
1556
1557
1558
1559
1560
1561
1562
1563
1564
1565
1566
1567
1568
1569
1570
1571
1572
1573
1574
1575
1576
1577
1578
1579
1580
1581
1582
1583
1584
1585
1586
1587
1588
1589
1590
1591
1592
1593
1594
1595
1596
1597
1598
1599
1600
1601
1602
1603
1604
1605
1606
1607
1608
1609
1610
1611
1612
1613
1614
1615
1616
1617
1618
1619
1620
1621
1622
1623
1624
1625
1626
1627
1628
1629
1630
1631
1632
1633
1634
1635
1636
1637
1638
1639
1640
1641
1642
1643
1644
1645
1646
1647
1648
1649
1650
1651
1652
1653
1654
1655
1656
1657
1658
1659
1660
1661
1662
1663
1664
1665
1666
1667
1668
1669
1670
1671
1672
1673
1674
1675
1676
1677
1678
1679
1680
1681
1682
1683
1684
1685
1686
1687
1688
1689
1690
1691
1692
1693
1694
1695
1696
1697
1698
1699
1700
1701
1702
1703
1704
1705
1706
1707
1708
1709
1710
1711
1712
1713
1714
1715
1716
1717
1718
1719
1720
1721
1722
1723
1724
1725
1726
1727
1728
1729
1730
1731
1732
1733
1734
1735
1736
1737
1738
1739
1740
1741
1742
1743
1744
1745
1746
1747
1748
1749
1750
1751
1752
1753
1754
1755
1756
1757
1758
1759
1760
1761
1762
1763
1764
1765
1766
1767
1768
1769
1770
1771
1772
1773
1774
1775
1776
1777
1778
1779
1780
1781
1782
1783
1784
1785
1786
1787
1788
1789
1790
1791
1792
1793
1794
1795
1796
1797
1798
1799
1800
1801
1802
1803
1804
1805
1806
1807
1808
1809
1810
1811
1812
1813
1814
1815
1816
1817
1818
1819
1820
1821
1822
1823
1824
1825
1826
1827
1828
1829
1830
1831
1832
1833
1834
1835
1836
1837
1838
1839
1840
1841
1842
1843
1844
1845
1846
1847
1848
1849
1850
1851
1852
1853
1854
1855
1856
1857
1858
1859
1860
1861
1862
1863
1864
1865
1866
1867
1868
1869
1870
1871
1872
1873
1874
1875
1876
1877
1878
1879
1880
1881
1882
1883
1884
1885
1886
1887
1888
1889
1890
1891
1892
1893
1894
1895
1896
1897
1898
1899
1900
1901
1902
1903
1904
1905
1906
1907
1908
1909
1910
1911
1912
1913
1914
1915
1916
1917
1918
1919
1920
1921
1922
1923
1924
1925
1926
1927
1928
1929
1930
1931
1932
1933
1934
1935
1936
1937
1938
1939
1940
1941
1942
1943
1944
1945
1946
1947
1948
1949
1950
1951
1952
1953
1954
1955
1956
1957
1958
1959
1960
1961
1962
1963
1964
1965
1966
1967
1968
1969
1970
1971
1972
1973
1974
1975
1976
1977
1978
1979
1980
1981
1982
1983
1984
1985
1986
1987
1988
1989
1990
1991
1992
1993
1994
1995
1996
1997
1998
1999
2000
2001
2002
2003
2004
2005
2006
2007
2008
2009
2010
2011
2012
2013
2014
2015
2016
2017
2018
2019
2020
2021
2022
2023
2024
2025
2026
2027
2028
2029
2030
2031
2032
2033
2034
2035
2036
2037
2038
2039
2040
2041
2042
2043
2044
2045
2046
2047
2048
2049
2050
2051
2052
2053
2054
2055
2056
2057
2058
2059
2060
2061
2062
2063
2064
2065
2066
2067
2068
2069
2070
2071
2072
2073
2074
2075
2076
2077
2078
2079
2080
2081
2082
2083
2084
2085
2086
2087
2088
2089
2090
2091
2092
2093
2094
2095
2096
2097
2098
2099
2100
2101
2102
2103
2104
2105
2106
2107
2108
2109
2110
2111
2112
2113
2114
2115
2116
2117
2118
2119
2120
2121
2122
2123
2124
2125
2126
2127
2128
2129
2130
2131
2132
2133
2134
2135
2136
2137
2138
2139
2140
2141
2142
2143
2144
2145
2146
2147
2148
2149
2150
2151
2152
2153
2154
2155
2156
2157
2158
2159
2160
2161
2162
2163
2164
2165
2166
2167
2168
2169
2170
2171
2172
2173
2174
2175
2176
2177
21

Acknowledgements

I want to thank my thesis advisor Dr Byron M. Welsh for his guidance during this thesis project. I also want to thank the members of the 6585 Test Group, Radar Target Scattering Division, for suggesting this topic and providing the financial resources necessary to complete this thesis.

I am grateful to my classmates for their friendship and help throughout our many classes. I am especially grateful to my wife Alicia who supported me every way she possibly could throughout the thesis effort.

Alan L. Buterbaugh

Table of Contents

| | Page |
|--|---------|
| Table of Contents | iii |
| List of Figures | vi |
| List of Tables | vii |
| Abstract | viii |
| I. Introduction | 1-1 |
| 1.1 Background | 1-1 |
| 1.2 Goals | 1-3 |
| 1.3 Approach | 1-3 |
| II. Radar Detection Calculations | 2-1 |
| 2.1 Pulsed Radar Receiver Model | 2-1 |
| 2.1.1 Neyman-Pearson Detection Criteria | 2-3 |
| 2.2 Swerling Fluctuation Models | 2-4 |
| 2.2.1 Swerling Models | 2-5 |
| 2.3 Partially Correlated Radar Pulses | 2-7 |
| 2.4 Signal Covariance Matrix and Eigenvalues | 2-9 |
| 2.5 Calculating P_D Using Contour Integration | 2-13 |
| 2.5.1 Saddlepoint Integration of $q_{\pm}(V_T)$ | 2-15 |
| 2.6 Detection Calculations | 2-17 |
| 2.6.1 Detection Threshold V_T | 2-17 |
| 2.6.2 Covariance Matrix C | 2-18 |
| 2.6.3 Determination of C Eigenvalues λ_i | 2-18 |

| | Page |
|--|------|
| 2.6.4 Calculation of P_D | 2-19 |
| 2.6.5 Kanter Results | 2-19 |
| 2.6.6 Saddlepoint Integration Method | 2-19 |
| 2.6.7 Summary | 2-23 |
| III. Determination of the Target Autocovariance | 3-1 |
| 3.1 Autocovariance of a Complex Target | 3-1 |
| 3.1.1 Assumptions | 3-4 |
| 3.1.2 Implications | 3-4 |
| 3.1.3 Point Source Scattering Centers | 3-7 |
| 3.1.4 Uniform Distribution of Scattering Centers | 3-9 |
| 3.2 Empirical Estimate of the Autocorrelation Function | 3-10 |
| 3.3 Summary | 3-10 |
| IV. Target Model | 4-1 |
| 4.1 AIM-9 Missile | 4-1 |
| 4.2 AIM-9 Missile Autocovariance Predictions | 4-4 |
| 4.3 Autocovariance of the AIM-9 Missile at 30, 40, and 45 degrees | 4-7 |
| 4.4 Autocovariance of the AIM-9 Missile at 0, 10, and 30 degrees | 4-9 |
| 4.5 Summary | 4-12 |
| V. Concluding Examples | 5-1 |
| VI. Conclusions | 6-1 |
| 6.1 Follow-on Efforts | 6-1 |
| Appendix A. Derivation of $L(s)$ | A-1 |

| | |
|--|--------|
| | Page |
| Appendix B. Determination of the Exponential Covariance Matrix Eigen- values | B-1 |
| Bibliography | BIB-1 |
| Vita | VITA-1 |

List of Figures

| Figure | Page |
|--|------|
| 2.1. Radar Receiver Block Diagram | 2-2 |
| 2.2. Detector Output pdf | 2-3 |
| 2.3. Kanter's Method for $N = 30$ pulses integrated | 2-20 |
| 2.4. Saddlepoint Integration for 30 radar pulses | 2-22 |
| 2.5. Saddlepoint Integration for 150 radar pulses | 2-22 |
| 3.1. Target/Observer Geometry | 3-3 |
| 4.1. AIM-9 Missile | 4-2 |
| 4.2. 36 GHz, $0^\circ - 180^\circ$ Missile RCS Azimuth Plot | 4-2 |
| 4.3. 36 GHz, $30^\circ - 60^\circ$ Missile RCS Azimuth Plot | 4-3 |
| 4.4. Scattering Center Locations at a 45° Observation Angle | 4-5 |
| 4.5. Predicted and Measured RCS Azimuth Patterns | 4-6 |
| 4.6. Signal Autocovariance, 30 deg off Nose, 5 Scatters | 4-7 |
| 4.7. Signal Autocovariance, 40 deg off Nose | 4-8 |
| 4.8. Signal Autocovariance, 45 deg off Nose | 4-8 |
| 4.9. Signal Autocovariance, 0 deg off Nose | 4-10 |
| 4.10. Signal Autocovariance, 10 deg off Nose | 4-10 |
| 4.11. Signal Autocovariance, 30 deg off Nose, 15 Scatters | 4-11 |
| 5.1. Missile/Radar Engagement Geometry | 5-1 |
| 5.2. Missile RCS Azimuth Plot | 5-3 |
| 5.3. Autocovariance for 30 Degrees off Nose | 5-3 |
| 5.4. Pd for 1 sec Observation Time | 5-4 |
| 5.5. Pd for 3 sec Observation Time | 5-5 |
| 5.6. Pd for 3.75 sec Observation Time | 5-5 |

List of Tables

| Table | Page |
|---|------|
| 2.1. Swerling Fluctuation Models | 2-5 |
| 4.1. Locations of the Scattering centers at a 45° Observation Angle . | 4-4 |
| 4.2. Locations of the Scattering centers at a 0° Observation Angle . . | 4-9 |

Abstract

This thesis provides a method for determining the detection of partially correlated Rayleigh distributed radar returns by a pulsed search radar. The receiver consists of a quadrature demodulator receiver, followed by a square law envelope detector and a linear post-detection integrator. In addition, a technique for determining the pulse-to-pulse correlation of a complex target is given using inverse Fourier transforms of the target scattering centers. An AIM-9 missile is used to illustrate how the partially correlated detection techniques and the pulse-to-pulse correlation predictions can be used to determine the probability of detection.

THE DETECTION AND CORRELATION MODELING OF RAYLEIGH DISTRIBUTED RADAR SIGNALS

I. Introduction

1.1 Background

One of the major areas of interest in the development of military aircraft systems is the radar power reflected or scattered from an aircraft when it is illuminated by a radar. The measure of this scattered power is called the radar cross section (RCS). The RCS of an aircraft is typically measured in 0.1° azimuth samples for a given elevation angle. At radar frequencies greater than 8 GHz the highly fluctuating RCS may be under-sampled and an accurate characterization of the RCS may not be achieved. Increasing the angular sampling rate will give a more detailed characterization of the RCS; however, the cost required to upgrade the measurement systems to achieve the smaller angular samples is high. The additional information obtained from improved sampling may be of marginal value when compared to the price required to upgrade the measurement system.

If we are interested in an exact deterministic characterization of the target's RCS, then we would nominally need a sampling rate to support at least two samples for every lobe. This criteria is impossible to achieve for complex targets due to the highly fluctuating nature of the RCS pattern. The term complex refers to the type of scattering expected from a target consisting of many scattering centers. In addition, due to the dynamic nature of the aircraft/radar engagement it is not possible to completely characterize the RCS deterministically for every possible observation

angle. A complete characterization of the RCS would require both the azimuth and elevation RCS data in very small increments, i.e. on the order of tenths of a degree for typical targets. Even if we did measure the RCS at all angles of interest, it would not be feasible to handle this huge amount of data, and the data would most likely be reduced or compressed via statistical processing techniques.

Given that a deterministic method for characterizing the RCS is not feasible for the complex target, a statistical approach is considered. The key ingredients in a statistical characterization is the RCS probability density function and the second order moment of the RCS. The second order moment describes how the RCS is expected to fluctuate from a particular observation angle to another observation angle. If we are interested in characterizing how the RCS fluctuations affect the probability of detection, then we need to know how the second order moment of the RCS affects the pulse-to-pulse correlation of the received return signal and how this pulse-to-pulse correlation affects the probability of detection. The purpose of this thesis is to investigate how the RCS fluctuations affect the pulse-to-pulse correlation of the received signal. With this purpose in mind, two questions naturally arise. The first is how important is the pulse-to-pulse correlation of the reflected radar signal in determining the detection of the target? The second question is if the pulse-to-pulse correlation is important, how do we determine the correlation properties for a given target? The first question can be answered by quantifying how the pulse-to-pulse correlation properties of the RCS affect target detectability. The second question can be answered by developing analytic models which describe the target fluctuations. Unfortunately, there has only been a limited amount of work performed on the correlated nature of radar return signals. Thus, before we can answer the angular sampling question, we must develop a partially correlated radar detection model and determine a method for predicting the signal correlation parameters.

1.2 Goals

The primary goal of this thesis is to investigate the importance of the pulse-to-pulse correlation of the radar returns on the probability of detection (P_D). The second goal is to determine a method for predicting the pulse-to-pulse correlation characteristic without explicitly making the required detailed measurements.

1.3 Approach

In order to understand how the pulse-to-pulse correlation affects the target detectability, a detection model is developed that explicitly incorporates the effects of pulse-to-pulse correlation. Chapter 2 introduces the radar receiver system used to investigate the detection of partially correlated return signals. The radar receiver model consists of a quadrature demodulator receiver, followed by a square law envelope detector and a linear post-detection integrator. The Neyman-Pearson detection criteria is used to determine the probability of detection. Using the Neyman-Pearson criteria, four techniques for calculating the probability of detection of a target by a pulsed search radar are introduced. I will then use these techniques to investigate the importance of the pulse-to-pulse correlation of the received signal in determining P_D of the target.

Once the importance of the pulse-to-pulse correlation on P_D is shown, it is necessary to establish a method for predicting this correlation characteristic. Chapter 3 develops the analytic models to predict this pulse-to-pulse correlation. After the analytic correlation models are developed, it will be possible to determine the target detectability using the detection techniques of chapter 2. Using the results from the general correlation models, we will generate the target autocorrelation function of two different distributions of the RCS scattering centers. The final section of this chapter gives an empirical approach for estimating the pulse-to-pulse correlation using measured RCS data.

Having an understanding of the importance of the affects of the pulse-to-pulse correlation properties in chapter 3, I seek to develop a method to actually predict these properties for a complex target. Chapter 4 illustrates how these properties can be predicted for an AIM-9 missile. Finally, chapter 5 illustrates how the correlation models and the radar detection technique of chapter 2 are used to determine the probability of detection for a given radar/aircraft engagement.

II. Radar Detection Calculations

Developing a radar detection model is the first step required to investigate how the target RCS fluctuations affect the detectability of a target. Pulsed radar systems typically integrate tens to hundreds of pulses to improve the detection probability. The process of summing all the radar return pulses for the purpose of improving detection is called integration (17). For the pulsed radar system integrators we want to know the importance of the pulse-to-pulse correlation in calculating P_D .

This chapter introduces the radar receiver system and the Neyman-Pearson detection criteria used to determine the probability of detection. Four techniques for calculating the probability of detection by a pulsed search radar are then introduced. The first technique is based on the early work of Peter Swerling (19). While this technique does not incorporate the pulse-to-pulse correlation properties of the radar return, it is included since it has become a virtual “standard” for calculating radar detection ranges for high frequency radar systems. The Swerling results are also useful as a baseline to compare with the other calculations. The second detection calculation technique is also developed by Swerling (18). The pulse-to-pulse correlation is modeled in the received signal covariance matrix and P_D is determined by the eigenvalues of this matrix. The signal covariance matrix and eigenvalues are describe in section 2.3. Next, Irving Kanter’s (14) technique for determining the eigenvalues of the signal covariance matrix is introduced. Unfortunately, summation errors associated with this technique limit the number of integrated pulses to less than 30. The final detection technique, by Carl Helstrom (12), solves the summation error problem through the use of contour and saddlepoint integration techniques.

2.1 Pulsed Radar Receiver Model

The radar receiver model consists of a quadrature demodulator receiver, followed by a square law envelope detector and a linear post-detection integrator. A

block diagram of the receiver structure is given in Fig 2.1. This receiver represents the optimum detection receiver structure for small signal-to-noise ratio signals (5).

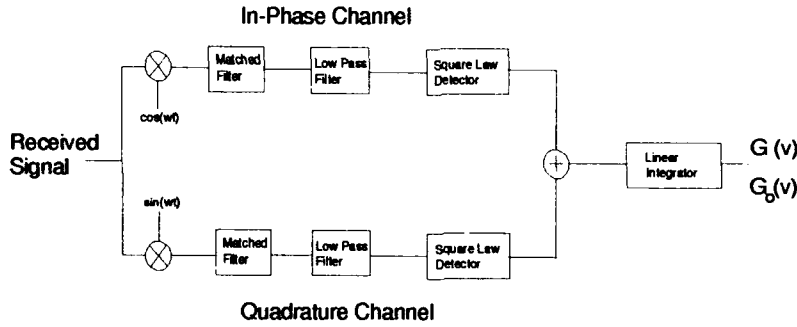


Figure 2.1. Radar Receiver Block Diagram

The radar receiver noise is assumed to be additive, zero mean Gaussian. We will also assume that the envelope of each pulse out of the square law detector is sampled at a time when the received signal is expected to peak in the absence of noise. This sampling is then repeated for each of the N received pulses. Let the detector output for each pulse be normalized by the receiver noise power, $2\beta^2$. The normalized output from the integrators for N pulses is

$$v = \frac{1}{2\beta^2} \sum_{i=1}^N z_i, \quad z_i = |x_i + jy_i|^2 \quad (2.1)$$

where x_i and y_i are the in-phase and quadrature phase signals of the i th pulse through the square law detectors.

The following notation will be used to defined the various quantities used in this chapter. Hypothesis H_1 is used to represent the condition when the received signal consists of the target return plus noise, and hypothesis H_o represents the condition where noise alone is present. $G(v)$ is used to represent the integrator output probability density function (pdf) of the N received signals for the H_1 hypothesis, and $G_o(v)$ represents the output for the H_o hypothesis. Figure 2.2 illustrates a

representative example of the integrator output pdf's $G(v)$ and $G_o(v)$. Additionally,

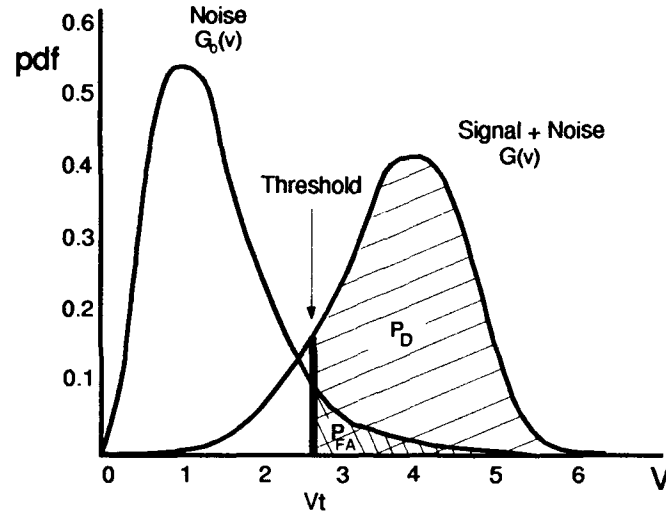


Figure 2.2. Detector Output pdf

we will define the per pulse ratio of signal power to average noise power by

$$\chi \doteq \frac{\bar{z}}{2\beta^2}, \quad (2.2)$$

where \bar{z} is the mean value of the received signal through the detectors.

2.1.1 Neyman-Pearson Detection Criteria The Neyman-Pearson detection criteria, which is most often used in radar, maximizes the detection probability for a fixed probability of false alarm, P_{FA} . Using the Neyman-Pearson criteria, the detection threshold, (V_T) is determined by the pdf of the noise only signal, $G_o(v)$, and the desired P_{FA} . The P_{FA} is calculated by integrating $G_o(v)$ from V_T to infinity. Once the threshold has been determined, the probability of detection is calculated by integrating the signal plus noise conditional pdf, $G(v)$ from V_T to infinity. These quantities are explicitly given by:

$$P_{FA} = \int_{V_t}^{\infty} G_o(v) dv \quad (2.3)$$

$$P_D = \int_{V_t}^{\infty} G(v) dv \quad (2.4)$$

Solving for the threshold level, V_T , is relatively easy if the system noise has a Gaussian distribution. For this case P_{FA} can easily be written as (14)

$$P_{FA} = e^{-V_t} \sum_{n=0}^{N-1} \frac{V_T^n}{n!}. \quad (2.5)$$

Determining the P_D is difficult, since the pdf of the integrator output statistic, $G(v)$, depends on the fluctuating radar return signal and the pulse-to-pulse correlation properties. These fluctuations and the pulse-to-pulse correlation properties in turn depend on the target's RCS, the movement of the aircraft or radar within the N pulse integration period, and the radar's pulse repetition frequency (prf). The first attempt at calculating the P_D is to simply assume a form for $G(v)$, and model the individual return pulses as being either completely correlated or completely uncorrelated. This assumption greatly simplifies the mathematics involved and allows us to calculate P_D in an easy manner.

2.2 *Swerling Fluctuation Models*

The first technique we will consider for calculating the P_D was developed by Peter Swerling (19). The resulting models developed using this technique are the most commonly used to predict the target detection probability. Swerling (19) uses two target model pdf's $p(z)$ to describe the pulse signal fluctuations through the square law detector. These two fluctuation models describe the signal amplitude fluctuations and have been found to correspond to many types of targets. The first pdf studied by Swerling is expressed by the Rayleigh distribution (negative-exponential),

$$p(z) = \frac{1}{z} \exp\left(-\frac{z}{z}\right), \quad z \geq 0, \quad (2.6)$$

where z is the input signal power and \bar{z} is the average signal power. The second target pdf studied by Swerling is given as a chi-square distribution,

$$p(z) = \frac{4z}{\bar{z}^2} \exp\left(-\frac{2z}{\bar{z}}\right), \quad z \geq 0. \quad (2.7)$$

In addition to the two target pdf's, Swerling assumes two types of signal fluctuations from one pulse to the next pulse. In the first case, the signal amplitude is assumed to be completely correlated for each pulse within a single scan of the radar. For the second case, the pulses are assumed to be un-correlated from pulse-to-pulse. The two target fluctuation pdf's and the two pulse-to-pulse fluctuation models are combined to yield the four well known Swerling fluctuation models used in detectability studies. The four models are shown in Table 2.1.

Table 2.1. Swerling Fluctuation Models

| Target pdf | Scan-to-Scan Signal Fluctuations | Pulse-to-Pulse Signal Fluctuations |
|--|-------------------------------------|---------------------------------------|
| $p(z) = \frac{1}{\bar{z}} \exp\left(-\frac{z}{\bar{z}}\right)$ | SW1 | SW2 |
| $p(z) = \frac{4z}{\bar{z}^2} \exp\left(-\frac{2z}{\bar{z}}\right)$ | SW3 | SW4 |

2.2.1 Swerling Models Deciding which Swerling model to use in a detectability study depends on the target's RCS scintillation characteristics, and on the pulse repetition frequency (prf) of the radar. If the target can be represented as a collection of many independently fluctuating reflectors of approximately equal magnitude, then the pdf of the detector output is close to the Rayleigh pdf given in eqn 2.6. Experimentally it has been shown that if the number of reflectors is as small as four or five the pdf can still be approximated by this pdf. Targets which can be represented

as one large reflector with a number of smaller reflectors are more appropriately modeled with the pdf in eqn 2.7 (8).

The choice of scan-to-scan or pulse-to-pulse fluctuations is determined by the radar's prf and the RCS characteristics of the target. The scan-to-scan model applies to jet aircraft or missiles where the phase scattering centers may be moving slowly compared to the radar's prf. Pulse-to-pulse fluctuations would apply to propeller-driven aircraft if the propellers contribute a large portion of the echoing area, or if the engine components are within the radar's line-of-sight. Targets for which very small changes in orientation would mean large changes in cross section, or targets viewed by a radar with sufficiently low pulse repetition rates would also be modeled with a pulse-to-pulse signal fluctuation model (8).

In the later investigation of the effects of partial pulse-to-pulse correlation we are restricted to Rayleigh distributions for the square law detector output z . Therefore, we will only concentrate on the *SW1* and *SW2* detection models. A simple form for P_D for N un-correlated return signals, *SW2*, is given by Irving Kanter (14) as:

$$P_D = \exp\left(-\frac{V_T}{1+\chi}\right) \sum_{n=0}^{N-1} \left[\frac{V_T}{1+\chi}\right]^n \frac{1}{n!} \quad (2.8)$$

Similarly, for completely correlated return signals, *SW1*, P_D is given by:

$$P_D = P_{FA} + \frac{e^{-V_T}}{1+N\chi} \sum_{n=1}^{\infty} \left(\frac{N\chi}{1+N\chi}\right)^n \sum_{k=N}^{N-1+n} \frac{V_T^k}{k!} \quad (2.9)$$

The Swerling models are virtually a "standard" for radar detection-range calculations (2) and provide a baseline to compare to the partially correlated detection models. Difranco and Rubin (5) provide a good description on the use and selection of the proper Swerling models for detectability studies.

2.3 Partially Correlated Radar Pulses

The Swerling models are important since they are the most widely used models in radar detection studies; however, these four models consider only the cases where the signal is either completely correlated (*SW1* and *SW3*) or completely uncorrelated (*SW2* and *SW4*) from pulse-to-pulse. Continuing his early development, Swerling (18) extended his detection theory to the more general case of partially correlated radar return pulses. Recall that the probability of detection, P_D , and probability false alarm, P_{FA} , are given by

$$P_{FA} = \int_{V_t}^{\infty} G_o(v) dv = e^{-V_t} \sum_{n=0}^{N-1} \frac{V_t^n}{n!}$$

$$P_D = \int_{V_t}^{\infty} G(v) dv,$$

and

$$v = \frac{1}{2\beta^2} \sum_{i=1}^N z_i, \quad z_i = |x_i + jy_i|^2,$$

where x_i and y_i are the in-phase and quadrature phase of the received signal and N is the number of integrated pulses. These components are assumed to be Gaussian random variables with zero mean. In addition, z_i is assumed to be statistically independent of the receiver noise. For the signal plus noise case, hypothesis H_1 , calculation of P_D is difficult, since the statistics of v depends on the fluctuating radar return signal and on the pulse-to-pulse correlation properties. These fluctuations and pulse-to-pulse correlation properties in turn depend on the radar's prf and the movement of the aircraft or radar within the N pulse integration period.

To calculate P_D , we begin by manipulating $G(v)$ into a form which can be easily integrated by taking the Laplace transform of $G(v)$ and simplifying the resulting equation. P_D can then be determined by taking the inverse Laplace transform of

this result and integrating $G(v)$ from V_T to infinity. Since the steps involved in simplifying the Laplace transform of $G(v)$ are numerous, only the results will be given here. The complete derivation which closely follows Swerling's paper (18) is given in Appendix A.

The Laplace transform, $L(s)$, of $G(v)$ is given as

$$L(s) = \int_0^{\infty} e^{-sv} G(v) dv. \quad (2.10)$$

After much manipulation, the simplified expression for the Laplace transform of $G(v)$ is given as

$$L(s) = \prod_{i=1}^N \frac{1}{1 + s(1 + \chi \lambda_i)}, \quad (2.11)$$

where λ_i is the i th eigenvalue of the signal covariance matrix C . The individual elements of the signal covariance matrix are given as

$$c_{i,j} = E[z_i z_j], \quad i = 1 \cdots N, \quad j = 1 \cdots N, \quad (2.12)$$

where $E[]$ is the expectation operator. As stated earlier, the pulse-to-pulse correlation is primarily due changes in the target RCS within the N pulse integration period. All of the pulse-to-pulse correlation information is contained by eqn 2.12 and the resulting covariance matrix, C .

P_D is then determined by taking the inverse Laplace transform of eqn 2.11 and integrating the resultant pdf from V_T to infinity. The inverse Laplace transform of eqn 2.11 gives the following simplified form for $G(v)$:

$$G(v) = \sum_{n=1}^N \prod_{\substack{k=1 \\ k \neq n}}^N \left[\left(1 - \frac{1 + \chi \lambda_k}{1 + \chi \lambda_n} \right) \right]^{-1} \frac{\exp\left[\frac{-v}{1 + \chi \lambda_n}\right]}{1 + \chi \lambda_n} \quad (2.13)$$

Integrating this pdf from V_T to infinity yields P_D , which after simplification can be written as:

$$P_D = \sum_{n=1}^N \prod_{\substack{k=1 \\ k \neq n}}^N \left[\left(1 - \frac{1 + \chi \lambda_k}{1 + \chi \lambda_n} \right) \right]^{-1} \exp \left(\frac{-V_T}{1 + \chi \lambda_n} \right). \quad (2.14)$$

Equation 2.14 gives the desired P_D for a Rayleigh distributed signal, assuming the eigenvalues of the signal covariance matrix are known. While this technique is relatively straight forward, it is difficult to use because of the need to determine the N eigenvalues of a N by N signal covariance matrix. The difficulty of computing the covariance matrix eigenvalues can be overcome by a technique developed by Irving Kanter (14) discussed in the next section.

2.4 Signal Covariance Matrix and Eigenvalues

The third technique for calculating the probability of detection of Rayleigh distributed radar returns is given by Irving Kanter (14). Kanter also addresses how to calculate the inverse Laplace transform of $L(s)$, and how to determine the eigenvalues of the covariance matrix. An alternative technique for calculating $L(s)$ is used, but the same results as determined by Swerling in eqn 2.11 are obtained. The technique of computing the signal covariance matrix eigenvalues introduced by Kanter allows us to easily determine P_D .

This section closely follows the work of Kanter (14) and shows how the covariance matrix eigenvalues are determined. We begin by first considering the nature of the received signal covariance matrix. If the received radar pulses arise from a stationary process, then the signal covariance matrix, C , will be a symmetric Toeplitz matrix with N distinct elements (14). With this observation in mind, we will assume that the received signal may be described by a first order Markov process. The justification for this assumption is based on target fluctuation characteristics observed by Barton (1), and on flight test measurements conducted by Edrington(7) which showed the detector output to be exponentially correlated for three different types

of aircraft. Using this assumption, P_D is determined from the eigenvalues of the signal covariance matrix which is characterized by a single correlation parameter ρ . Using these observations, the c_{kn} element of the covariance matrix, for a train of N uniformly spaced pulses, is given by

$$c_{kn} \doteq \rho^{|k-n|} \quad 0 \leq \rho \leq 1, \quad (2.15)$$

and the resulting signal covariance matrix is

$$C = \begin{bmatrix} 1 & \rho & \cdots & \rho^{N-1} \\ \rho & 1 & \rho & \vdots \\ \vdots & \ddots & \ddots & \rho \\ \rho^{N-1} & \cdots & \rho & 1 \end{bmatrix} \quad (2.16)$$

The eigenvalues of C provide a nontrivial solution to the matrix equation

$$[C - \lambda I]U = 0 \quad (2.17)$$

where I is an N by N identity matrix and U is a N dimensional vector with individual elements u_0, \dots, u_{N-1} . In addition, the sum of the eigenvalues equals the trace of C giving the relation

$$\sum_{i=1}^N \lambda_n = N, \quad (2.18)$$

which will be used later on.

As an example, consider the special case where the interpulse spacing is so large that the correlation of non-consecutive pulses may be neglected. For this case, the signal covariance matrix is tridiagonal and eqn 2.17 is equivalent to a homogeneous boundary value problem (14), which can be expressed as a set of homogeneous second

order difference equations of the form

$$\rho u_{n-1} + (1 - \lambda)u_n + \rho u_{n+1} = 0, \quad n = 1, \dots, N, \quad (2.19)$$

with the homogeneous boundary conditions,

$$u_0 = u_{N+1} = 0. \quad (2.20)$$

Since eqn 2.19 is linear and has constant coefficients, there are two solutions of the form

$$u_n = \gamma^n, \quad (2.21)$$

where

$$\gamma = \frac{\lambda - 1}{2\rho} \pm \sqrt{\left(\frac{\lambda - 1}{2\rho}\right)^2 - 1}. \quad (2.22)$$

The condition $|(\lambda - 1)/2\rho| \geq 1$ implies either $\lambda \geq 1 + 2\rho$ or $\lambda \leq 1 - 2\rho$, each of which leads to a contradiction of eqn 2.18. Thus, we must have $|(\lambda - 1)/2\rho| < 1$, and γ can be expressed as $\gamma = e^{\pm j\theta}$. Using the identity, $e^{\pm j\theta} = \cos \theta \pm j \sin \theta$, the real part of eqn 2.22 can then be expressed as:

$$\cos \theta = \frac{\lambda - 1}{2\rho} \quad (2.23)$$

The general solution to eqn 2.19 in terms of $e^{\pm jn\theta}$ can be written as

$$u_n = K_1 \cos n\theta + K_2 \sin n\theta \quad (2.24)$$

Since the boundary condition $u_0 = 0$ must be satisfied, K_1 must equal zero. The second boundary, $u_{N+1} = 0$, allows us to solve the transcendental equation 2.24 for θ . Rewriting eqn 2.24 for $n = N + 1$ gives

$$u_{N+1} = K_2 \sin(N + 1)\theta = 0. \quad (2.25)$$

Equation 2.25 then yields the distinct θ_n values:

$$\theta_n = \frac{n}{N+1}\pi, \quad n = 1, \dots, N \quad (2.26)$$

Note that the θ_n 's are equally spaced in the open interval $(0, \pi)$. Equation 2.23 yields the N signal covariance matrix eigenvalues

$$1 - 2\rho < \lambda_n = 1 + 2\rho \cos \theta_n < 1 + 2\rho, \quad n = 1, \dots, N. \quad (2.27)$$

The following example of solving for the probability of detection using this technique, will help to clarify the steps involved. Consider the case of two integrated pulses. The covariance matrix is given as

$$C = \begin{bmatrix} 1 & \rho \\ \rho & 1 \end{bmatrix} \quad (2.28)$$

From eqn 2.26, $\theta_1 = \pi/3$ and $\theta_2 = 2\pi/3$. The eigenvalues are determined from eqn 2.27 and are given as

$$\lambda = 1 \pm \rho. \quad (2.29)$$

The probability of detection, P_D , from our earlier results eqn 2.14, is given as

$$P_D = \sum_{n=1}^2 \prod_{\substack{k=1 \\ k \neq n}}^2 \left[1 - \frac{1 - \chi \lambda_k}{1 + \chi \lambda_n} \right]^{-1} \exp \left(-\frac{V_t}{1 + \chi \lambda_n} \right), \quad (2.30)$$

where V_T is the signal threshold required for a given P_{FA} and χ is the per pulse ratio of signal power to average noise power, and $\lambda_{1,2} = 1 \pm \rho$. Substituting in the eigenvalues and simplifying, results in the P_D given by

$$P_D = \exp \left\{ \frac{-(1 + \chi)V_T}{(1 + \chi)^2 - (\rho\chi)^2} \right\} * \left[\frac{1 + \chi}{\rho\chi} \sinh \left(\frac{\rho\chi V_T}{(1 + \chi)^2 - (\rho\chi)^2} \right) + \cosh \left(\frac{\rho\chi V_T}{(1 + \chi)^2 - (\rho\chi)^2} \right) \right]$$

This result agrees with the value calculated by Schwartz (16) for two integrated pulses. For the case where the correlation of non-consecutive pulses may not be ignored, a similar technique of formulating and solving an equivalent homogeneous boundary value problem may be applied. Since this is the case more frequently encountered, the derivation given in Kanter's paper (14) is included in Appendix B.

Evaluating the P_D by this technique is difficult when $N > 30$, since the first terms in the series of eqn 2.14 are large when the eigenvalues are close together in magnitude, which will be the case when N is large. As shown in section 2.6.5, the summation errors associated with this technique become too large, and an alternative technique for determining P_D is required.

2.5 Calculating P_D Using Contour Integration

The final technique for determining the P_D of Rayleigh distributed signals is based on the work of Carl Helstrom (12). The difficulty of the summation errors of Kanter's technique can be avoided through the use of saddle-point integration and its associated saddlepoint approximations. The use of contour integration to determine P_D is also introduced in this section. The contour integration technique gives the same results for P_D given earlier; however, the notation is slightly different.

Before we introduce the saddlepoint integration techniques, we will first show how P_D can also be determined by contour integration. Recall from our earlier results that the Laplace transform of the detector output is given by

$$L(s) = \prod_{i=1}^N \frac{1}{1 + s(1 + \chi \lambda_i)} \quad (2.31)$$

Equation 2.31 and the resultant derivation can be simplified by defining α_k as:

$$\alpha_k \doteq 1 + \chi \lambda_k \quad (2.32)$$

Rewriting the Laplace transform of $G(v)$, eqn 2.31, in terms of α gives:

$$L(s) = \prod_{i=1}^N \frac{1}{1 + \alpha_k s} \quad (2.33)$$

As shown earlier, P_D is given as the integral of $G(v)$ from the threshold to infinity. In the two previous techniques, $G(v)$ was determined from the inverse Laplace transform of $L(s)$. P_D was then determined by integration of $G(v)$ over the appropriate limits. An alternative technique for calculating P_D is to transform the integration limits to the s -plane and perform the appropriate contour integration. This is the technique used by Helstrom (12). To use this technique, we begin with the moment-generating function, $h(s)$, of the statistic v . The moment-generating function is given by:

$$h(s) = E[e^{-sv}] = [D(s)]^{-1}, \quad (2.34)$$

where

$$D(s) = \prod_{k=1}^N (1 + \alpha_k s). \quad (2.35)$$

The cumulative distribution function, cdf, is the integral of $G(v)$ from 0 to V_T , which is equal to $1 - P_D$. The cdf is generated from the moment generating function $h(s)$ by the inverse Laplace transform of eqn 2.33 and is given by

$$q_-(V_T) = 1 - P_D = \int_{c-j\infty}^{c+j\infty} (s)^{-1} h(s) e^{sV_T} \frac{ds}{j2\pi}, \quad c > 0, \quad (2.36)$$

with integration along a straight vertical contour in the right half-plane. The complementary cumulative distribution function, ccdf, and the P_D are given as the integral of $G(v)$ from V_T to infinity. The ccdf is given by

$$q_+(V_T) = P_D = \int_{c-j\infty}^{c+j\infty} (-s)^{-1} h(s) e^{sV_T} \frac{ds}{j2\pi}, \quad c < 0, \quad (2.37)$$

with integration in the portion of the converging strip of the Laplace transform $h(s)$ in the left half-plane. The N poles of $h(s)$ lie at the points $s_k = \frac{-1}{\alpha_k}$, and $c > \frac{-1}{\alpha_1}$, where α_1 is the largest of the scaled eigenvalues of the C matrix. The residue theorem is then used to evaluate the P_D (10). The resultant P_D is given by

$$P_D = q_+(V_T) = \sum_{k=1}^N \prod_{\substack{n=1 \\ n \neq k}}^N \left[1 - \frac{\alpha_n}{\alpha_k}\right]^{-1} \exp\left(\frac{-V_T}{\alpha_k}\right). \quad (2.38)$$

This technique of determining the P_D gives the same results developed by Kanter (14) and Swerling (18), and it has the same limitations they encountered. Recall, the first terms in the series are large when the signal covariance matrix eigenvalues are of approximately the same magnitude. The ill behavior of the summation errors in eqn 2.38 can be avoided by evaluating eqn's 2.36 and 2.37 using saddlepoint integration and the corresponding saddlepoint approximations introduced by Helstrom (10).

2.5.1 Saddlepoint Integration of $q_{\pm}(V_T)$ The saddlepoint integration technique is described in detail in references (9),(10), and (11). The general approach to this technique starts with the integrals of the type described in eqn's 2.36 and 2.37 which have the form

$$q_{\pm}(V_T) = \int_{c-j\infty}^{c+j\infty} e^{\Phi(s)} \frac{ds}{j2\pi}, \quad (2.39)$$

where the "phase" term $\Phi(s)$ is given by the moment-generating function, eqn's 2.34 and 2.35, which when simplified results in

$$\Phi(s) = V_T s - \sum_{k=1}^N \ln(1 + \alpha_k s) - \ln(\mp s). \quad (2.40)$$

P_D is computed by deforming the contour of integration onto a path passing through the saddlepoint s_o^- or s_o^+ of the integrand of eqn 2.39 on the $\text{Re } s$ -axis. The saddle-

points are roots of the equation

$$\begin{aligned}\Phi'(s) &= V_T - \sum_{k=1}^N \alpha_k (1 + \alpha_k s)^{-1} - s^{-1} = 0, \\ s &= s_o^-, s_o^+, \quad -\alpha_1^{-1} < s_o^- < 0, \quad s_o^+ > 0.\end{aligned}\tag{2.41}$$

The roots of eqn 2.41 are computed using Newton's method where each trial value of s' is replaced by

$$s' \leftarrow s' - \frac{\Phi'(s')}{\Phi''(s')}\tag{2.42}$$

with

$$\Phi''(s) = \sum_{k=1}^N \alpha_k^2 (1 + \alpha_k s)^{-2} + s^{-2}.\tag{2.43}$$

The above procedure determines the saddlepoint s_o^+ or s_o^- . The cdf and ccdf are determined by the saddlepoint approximation:

$$q_{\pm}(V_T) \approx [2\pi\Phi''(s_o^{\mp})]^{-\frac{1}{2}} \exp(\Phi(s_o^{\mp}))\tag{2.44}$$

The probability of detection can be determined from either the cdf or the ccdf, and is given as

$$P_D = q_+(V_T) \approx [2\pi\Phi''(s_o^-)]^{-\frac{1}{2}} \exp(\Phi(s_o^-)).\tag{2.45}$$

$$P_D = 1 - q_-(V_T) \approx 1 - [2\pi\Phi''(s_o^+)]^{-\frac{1}{2}} \exp(\Phi(s_o^+)).\tag{2.46}$$

When $N \gg 1$ these approximations are adequate.

Now that we have a technique to determine P_D for correlated Rayleigh return signals, the next step is to use these models to show how P_D is determined for different covariance matrixes. In-addition, the next section will also show the summation error problem encountered by Irving Kanter.

2.6 Detection Calculations

This section discusses the actual calculation of P_D using the Kanter and Helstrom techniques described earlier. The detection calculation technique of Kanter (14) was implemented first. This method yields acceptable results for up to $N = 30$ pulses, and for correlation coefficients $\rho \leq 0.9$. For larger number of pulses and for higher correlation coefficients, the summation errors are too large. The technique of Helstrom (12) was implemented next to overcome this limitation. This technique yields acceptable results for all cases considered. For each technique the algorithms were written in FORTRAN 77 source code. The steps involved for calculating the probability of detection are:

Determine the detection threshold, V_T .

Calculate the covariance matrix, C , for N pulses.

Calculate the C matrix eigenvalues, λ_i .

Determine the probability of detection using eqn 2.14 or 2.45.

2.6.1 Detection Threshold V_T Recall, the detection threshold, V_T , is the required noise signal threshold to achieve a given P_{FA} . Unless otherwise specified this P_{FA} was set to 10^{-6} . Since the threshold is independent of the target signal, the threshold values are calculated in advance and stored in a data file. The following technique provides an effective way of calculating the threshold. An initial estimate of the threshold is given by (6),

$$V_T \approx \sqrt{N}\Phi^{-1}(P_{FA}) + N, \quad (2.47)$$

where $\Phi^{-1}(P_{FA})$ is a constant found on page 368 of Difrancio and Rubin (6). This approximation is valid for $10^{-2} \leq P_{FA} \leq 10^{-15}$ (6). A more accurate threshold is then calculated using our earlier results for P_{FA}

$$P_{FA} = e^{-V_T} \sum_{n=0}^{N-1} \frac{V_T^n}{n!}, \quad (2.48)$$

where V_T is varied and the calculated P_{FA} is compared to the desired value. When the difference is within an allowable limit, the threshold value, V_T , is written to the appropriate data file.

2.6.2 Covariance Matrix C With the appropriate value of V_T calculated for N pulses, the next step is calculate the covariance matrix. For the initial evaluation of this technique, an exponential correlation model described by Kanter (14) was used. For this case the received signal consists of a train of N pulses with uniform spacing between the individual pulses. The c_{kn} value of the covariance matrix are given as

$$c_{kn} \doteq \rho^{|k-n|}, \quad (2.49)$$

$$C = \begin{bmatrix} 1 & \rho & \rho^2 & \dots & \rho^{N-1} \\ \rho & 1 & \rho & \dots & \rho^{N-2} \\ \vdots & \ddots & \ddots & \ddots & \vdots \\ \rho^{N-2} & \dots & \rho & 1 & \rho \\ \rho^{N-1} & \dots & \rho^2 & \rho & 1 \end{bmatrix}. \quad (2.50)$$

2.6.3 Determination of C Eigenvalues λ_i The eigenvalues of the C matrix were determined using the IMSL DEVCSF FORTRAN subroutine (13). This subroutine determines the double precision eigenvalues for a real symmetric matrix using the method mentioned below.

Routine DEVCSF computes the eigenvalues and eigenvectors of a real symmetric matrix as follows: first, accumulating orthogonal similarity transformations are used to reduce the matrix to an equivalent symmetric tridiagonal matrix; second, the implicit QL algorithm is used to compute the eigenvalues and eigenvectors of this tridiagonal matrix. The

eigenvectors are normalized such that the ∞ -norm of each eigenvector is one (13).

The calculated eigenvalues were then compared to the eigenvalues calculated using Kanter's (14) technique. For the cases considered, the two techniques produced the same results.

2.6.4 Calculation of P_D The last step is to determine the P_D curves for various signal-to-noise ratios. Recall our earlier results for P_D was given as

$$P_D = \sum_{n=1}^N \prod_{\substack{k=1 \\ k \neq n}}^N \left[1 - \frac{1 - \chi \lambda_k}{1 + \chi \lambda_n} \right]^{-1} \exp \left[\frac{-V_t}{1 + \chi \lambda_n} \right], \quad (2.51)$$

where χ is the signal-to-noise ratio.

2.6.5 Kanter Results The above technique yields results which agree with the values calculated by Kanter (14). Unfortunately, as ρ approaches 1, or for $N \geq 30$ the summation errors become too large and the results become unacceptable for small signal-to-noise ratios. An illustration of these results are shown in Fig 2.3.

For $\rho = 0.8$ and $\rho = 0.9$, the summation error is too large. The magnitude of this error increases as the number of integrated pulses increases and/or as the correlation coefficient, ρ increases. Since this technique limits the number of pulses to be less than 30, this technique was abandoned for the Helstrom saddlepoint integration technique described in the next section.

2.6.6 Saddlepoint Integration Method The Helstrom technique is similar to the Kanter technique. The major difference is that saddlepoint integration techniques are utilized to perform the calculation of P_D (12). This integration technique avoids summation errors encountered with the Kanter technique. The algorithm developed in the previous section was used to determine the detection threshold V_T . The covariance matrix eigenvalues were also calculated by the technique described in

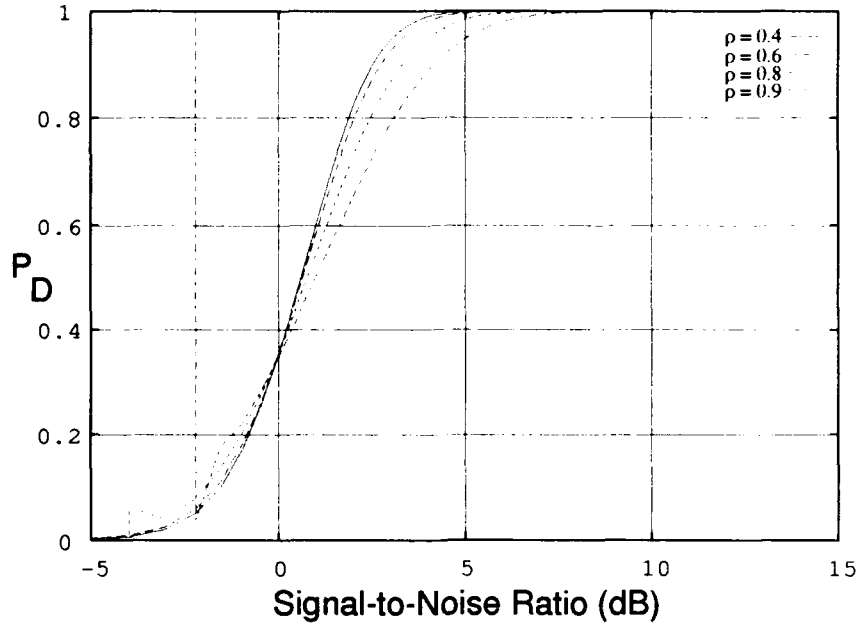


Figure 2.3. Kanter's Method for $N = 30$ pulses integrated

the previous section. A detailed discussion of the saddlepoint integration technique is given in chapter 2.

Recall the saddlepoints are roots of eqn 2.52 and are used to determine P_D .

$$\begin{aligned} \Phi'(s) &= V_T - \sum_{k=1}^N \alpha_k (1 + \alpha_k s)^{-1} - s^{-1} = 0, \\ s &= s_o^-, s_o^+, \quad -\alpha_k^{-1} < s_o^- < 0, \quad s_o^+ > 0 \end{aligned} \quad (2.52)$$

The saddlepoints are computed by Newton's method where each trial value of s' is replaced by

$$s' \leftarrow s' - \frac{\Phi'(s')}{\Phi''(s')} \quad (2.53)$$

with

$$\Phi''(s) = \sum_{k=1}^N \alpha_k^2 (1 + \alpha_k s)^{-2} + s^{-2}. \quad (2.54)$$

The above procedure determines the saddlepoint. The cdf and ccdf are determined using the saddlepoint approximation

$$q_{\pm}(V_T) \approx [2\pi\Phi''(s_o^{\mp})]^{-.5} \exp(\Phi(s_o^{\mp})). \quad (2.55)$$

The probability of detection can be determined from either the cdf or the ccdf by:

$$P_D = q_+(V_T) \approx [2\pi\Phi''(s_o^-)]^{-.5} \exp(\Phi(s_o^-)). \quad (2.56)$$

$$P_D = 1 - q_-(V_T) \approx 1 - [2\pi\Phi''(s_o^+)]^{-.5} \exp(\Phi(s_o^+)). \quad (2.57)$$

A plot of P_D using this technique for 30 pulses is shown in figure 2.4. As the figures demonstrate, the summation error associated with the earlier technique is avoided. Figure 2.5 shows the P_D curve for 150 pulses integrated. Again there are no noticeable anomalies associated with this technique even for highly correlated pulses.

Some observations about the results shown in Fig's 2.4 and 2.5 are useful. Smaller values of ρ correspond to signals which are less correlated, i.e. more fluctuating from pulse-to-pulse. For $P_D < 0.4$ the degree of correlation makes little difference, the more fluctuating signals are almost identical to the less fluctuating signals. Note that the $\rho = 0.4$ is close to the $\rho = 0.6$ curve, while the $\rho = 0.9$ is more spread out than $\rho = 0.95$. Having the curves that correspond to the higher fluctuating targets to the left of the less fluctuating curves implies the fluctuating targets require a lower signal-to-noise ratio to achieve a given P_D . Figure 2.4 shows the importance of the correlation properties in determining P_D . For a P_D of 0.95, the $\rho = 0.95$ correlation coefficient requires an additional signal-to-noise of 1.7 dB to achieve the same P_D as the $\rho = 0.4$ correlation coefficient.

The preceding analysis calculates P_D using an exponential correlation parameter. Recall that the exponential correlation parameter allows us to compute the

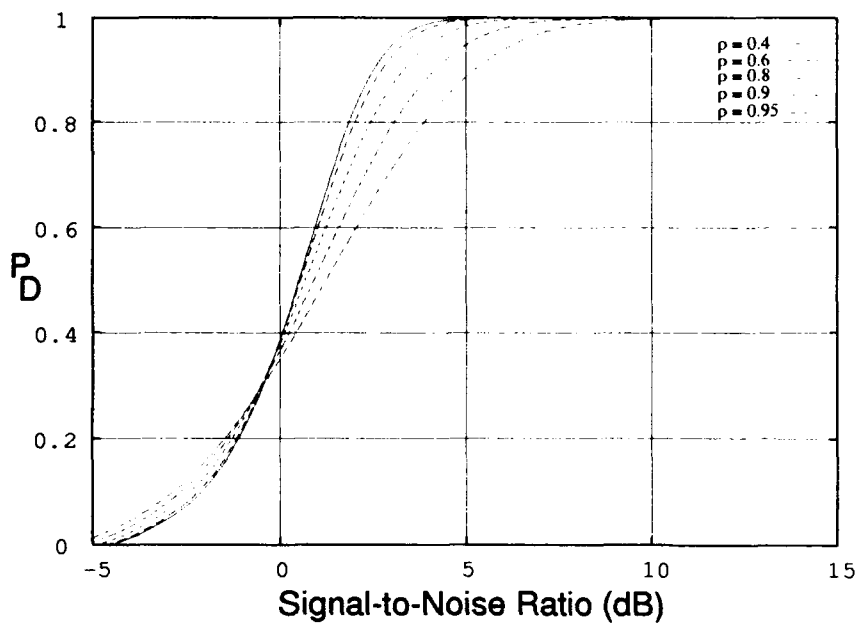


Figure 2.4. Saddlepoint Integration for 30 radar pulses

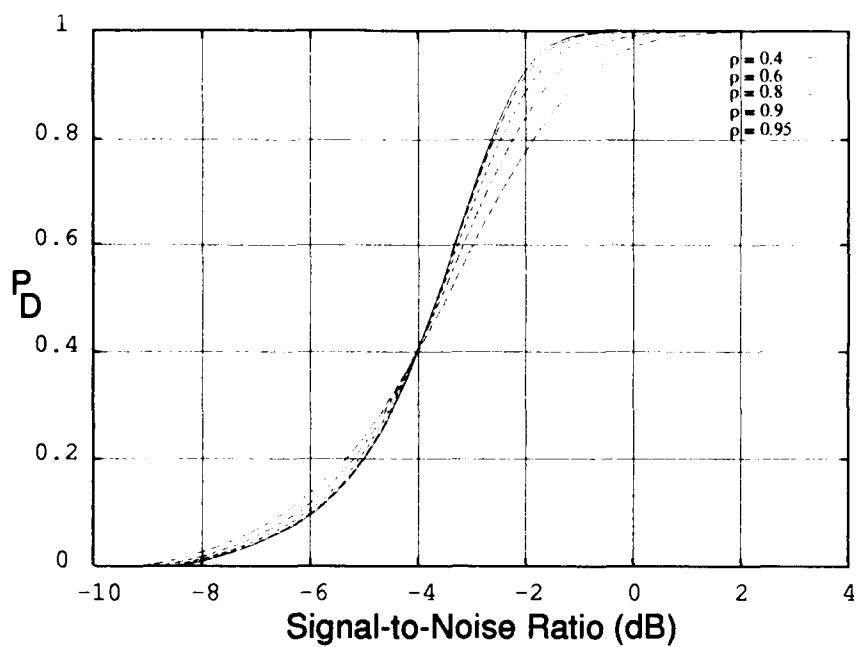


Figure 2.5. Saddlepoint Integration for 150 radar pulses

signal autocovariance matrix eigenvalues in a convenient manner. If the number of integrated pulses is less than 150 then the eigenvalues can also be determined by the IMSL fortran subroutine DEVCSF described in section 2.6.3. I used this subroutine to determine the covariance matrix eigenvalues with individual elements described by a $(\sin x/x)^2$ correlation parameter. P_D was then calculated with these eigenvalues and the results were compared to the P_D calculated with exponential parameter eigenvalues. The two different parameters yielded approximately the same P_D for all of the cases considered. This result indicates that P_D is primarily determined by how fast the correlation parameter first approaches zero and not on the behavior of the correlation parameter beyond this zero value.

2.6.7 Summary In this chapter we have introduced several techniques for determining the probability of detection of Rayleigh distributed radar returns. The original work of Peter Swerling (18) provides the theoretical background for determining P_D of partially correlated signals but does not provide an effective technique for calculating the required covariance matrix eigenvalues. A technique for determining the eigenvalues is given by Irving Kanter (14); however, summation errors limit the number of integrated pulses to 30. This limitation is corrected through the use of saddlepoint integration techniques introduced by Carl Helstrom (10). These models were then used to illustrate the importance of the correlation parameter ρ in determining P_D . For all the cases considered and for $P_D > 0.4$, the more fluctuating targets required a lower signal-to-noise ratio to achieve the same P_D . In addition, the results of this chapter shows that it is not possible to accurately determine P_D without considering the pulse-to-pulse correlation of the individual radar returns.

III. Determination of the Target Autocovariance

The pulse detection methods developed in chapter 2 require the pulse-to-pulse correlation of the received signal in order to generate the signal autocovariance matrix. Recall that the de-correlation of the signal may be caused by, among others, the target's rotation relative to the radar's line-of-sight or by changes in the radar frequency. The degree of correlation of the signal amplitude from one observation to the next will determine the detection probability (1). Several pdf's have been proposed to describe target fluctuation statistics (2). Among these are the chi-square family, the Rice family, the log-normal family, the Swerling models, and the Weinstock distributions. The Swerling's techniques described in chapter 2 (19) using completely correlated or completely un-correlated pulse-to-pulse signals can be applied to all the above models and for arbitrary pdf's, but extensive numerical calculations have been made only for the original Swerling pdf models. In addition, these calculations do not account for the pulse-to-pulse correlation of the received signal (2).

This chapter develops the analytic models to predict the autocovariance matrix of the received signal. Once the analytic models are developed, it will be possible to determine P_D using the results from the models and the prediction techniques of chapter 2. The first section develops a method of determining the signal autocorrelation function, and is based on the preliminary work of Byron Welsh, *et.al.* (20). Using the results from this model, we will generate the autocorrelation function for two different types of complex scattering targets. The final section of this chapter gives an empirical approach for estimating the autocovariance matrix.

3.1 Autocovariance of a Complex Target

The following results closely follow the preliminary work performed by Byron Welsh, *et.al.* (20) on RCS correlation modeling. Their work will permit us to develop the pulse-to-pulse autocorrelation function for an arbitrary distribution of scattering

centers. A spatial distribution of scatterers can be used to reproduce the scattering statistics expected from a complex target, where the term complex refers to the type of scattering expected from a target consisting of many scattering centers. The spatial extent of the scattering centers is assumed to be large compared to the wavelength of the incident electro-magnetic field. Since the spatial extent is large, the RCS aspect angle pattern will be highly fluctuating and the RCS statistics can be determined from the distribution of the scattering centers. In addition, the use of spatially distributed scatterers will allow us calculate the target autocovariance in a relatively simple manner. We will consider two spatial distribution of scatterers for this analysis. The first distribution is for a collection of scatterers where the individual scatterers have a Gaussian distribution about a set of fixed locations. This distribution requires detailed information about the target scattering centers and should accurately predict the target autocorrelation function. The second distribution considered is where the scattering centers are uniformly distribution within a rectangular box. This distribution was chosen since only the maximum target dimensions are required. These maximum dimensions correspond to the dimensions of the box. Since only the maximum dimensions are required, it is relatively easy to predict the autocovariance of the target using this distribution. Remember that we would like to predict the autocovariance using the simplest model possible. We will then compare the uniform distribution predictions to the point source distributions. If the two prediction methods agree, we will then be able to use the much simpler uniform distribution technique to calculate the target autocovariance.

The target and observer geometry used throughout this section is illustrated in Fig 3.1. The following definitions will be used through this section to describe the quantities of interest:

\vec{r}_i =vector position of the i th point scatterer

$\underline{b}_i(\hat{r})$ =scaler backscattered field from the i th point scatterer for a unit amplitude incident field

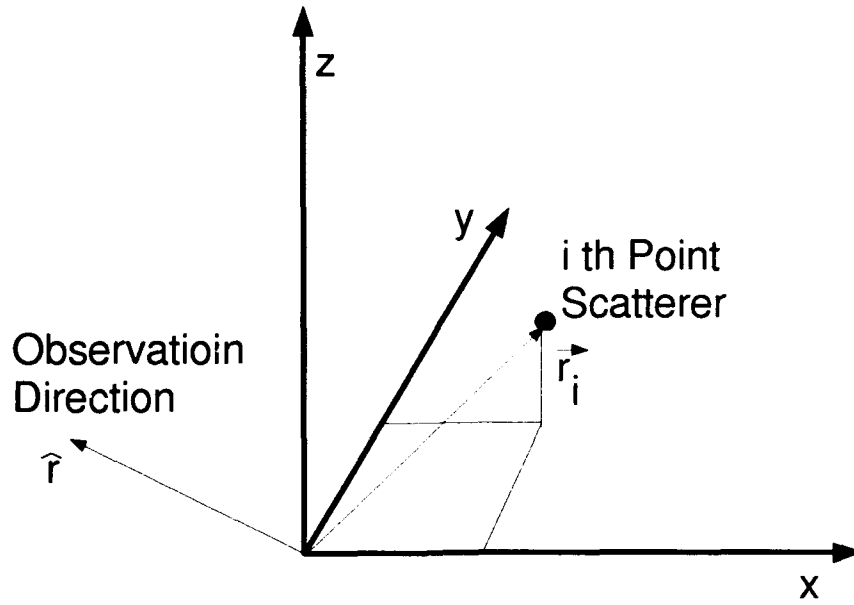


Figure 3.1. Target/Observer Geometry

\hat{r} = unit vector pointing in the direction of the observation point,

$\underline{y}(\hat{r})$ = complex amplitude of the total scattered E field,

λ = wavelength of the incident and scattered field.

The expression for the complex amplitude of the scattered field is given as

$$\underline{y}(\hat{r}) = \sum_{i=1}^N \underline{b}_i(\hat{r}) \exp \left\{ j \frac{4\pi}{\lambda} (\hat{r} \cdot \vec{r}_i) \right\}, \quad (3.1)$$

where N is the number of scatterers in the observation direction \hat{r} . The power of the scatterer field in the \hat{r} direction is proportional to the squared magnitude of the scattered field:

$$\sigma(\hat{r}) = |\underline{y}(\hat{r})|^2 = \sum_{i=1}^N \sum_{i'=1}^N \underline{b}_i(\hat{r}) \underline{b}_{i'}^*(\hat{r}) \exp \left\{ j \frac{4\pi}{\lambda} [\hat{r} \cdot (\vec{r}_i - \vec{r}_{i'})] \right\}. \quad (3.2)$$

The autocorrelation of σ is required to calculate P_D and is given as

$$\begin{aligned} R_\sigma(\hat{r}_1, \hat{r}_2) &= E[\sigma(\hat{r}_1)\sigma(\hat{r}_2)] \\ &= E[|\underline{y}(\hat{r}_1)|^2 |\underline{y}(\hat{r}_2)|^2] \end{aligned} \quad (3.3)$$

where $R_\sigma(\hat{r}_1, \hat{r}_2)$ is the autocorrelation function and $E[\]$ is the expected value operator. As will be discussed later, the individual elements of the signal covariance matrix C are generated from this autocovariance function.

3.1.1 Assumptions The following assumptions are made to simplify the analysis.

$$\underline{b}_i(\hat{r}) = \underline{b}_i.$$

$$|\underline{b}_i| \text{ is independent of } \arg[\underline{b}_i].$$

$$\arg[\underline{b}_i] \text{ is uniformly distributed over the interval } [0, 2\pi].$$

$$\underline{b}_i \text{ and } \vec{r}_i \text{ are independent.}$$

3.1.2 Implications The assumptions listed in the preceding section results in the following implications:

$$E[\underline{b}_i] = 0, \quad (3.4)$$

$$E[\underline{b}_i^2] = 0, \quad (3.5)$$

$$E[\underline{b}_i \underline{b}_{i'}^*] = \begin{cases} \alpha^2 & i = i', \\ 0 & i \neq i' \end{cases} \quad (3.6)$$

Using the above assumptions, the expected value of $\sigma(\hat{r})$ is given by

$$E[\sigma(\hat{r})] = N\alpha^2, \quad (3.7)$$

which agrees with the value determined by Crispin (3), for the incoherent addition of scatterers. Using the above assumptions, the autocorrelation function can be expressed as

$$R_{\sigma}(\hat{r}_1, \hat{r}_2) = E \left[\sum_{i=1}^N \sum_{i'=1}^N \sum_{n=1}^N \sum_{n'=1}^N \underline{b}_i \underline{b}_{i'}^* \underline{b}_n \underline{b}_{n'}^* \times \exp \left\{ j \frac{4\pi}{\lambda} [\hat{r}_1 \cdot (\vec{r}_i - \vec{r}_{i'}) + \hat{r}_2 \cdot (\vec{r}_n - \vec{r}_{n'})] \right\} \right].$$

Since \underline{b}_i and \vec{r}_i are independent, the quantity $E[\underline{b}_i \underline{b}_{i'}^* \underline{b}_n \underline{b}_{n'}^*]$ can be considered separately. Using eqn's 3.4 thru 3.6, it is easy to show:

$$E[\underline{b}_i \underline{b}_{i'}^*, \underline{b}_n \underline{b}_{n'}^*] = \begin{cases} E[|\underline{b}_i|^4] & i = i' = n = n' \\ \alpha^4 & i = i' \text{ and } n = n' \text{ and } i \neq n \\ \alpha^4 & i = n' \text{ and } n = i' \text{ and } i \neq i' \\ 0 & \text{otherwise} \end{cases} \quad (3.8)$$

Using eqn 3.8, the autocorrelation function can be written as:

$$\begin{aligned} R_{\sigma}(\hat{r}_1, \hat{r}_2) &= NE[|\underline{b}_i|^4] + N^2\alpha^4 - 2N\alpha^4 \\ &+ \alpha^4 \sum_{i=1}^N \sum_{i'=1}^N \left\{ E \left[\exp \left\{ j \frac{4\pi}{\lambda} [(\hat{r}_1 - \hat{r}_2) \cdot (\vec{r}_i - \vec{r}_{i'})] \right\} \right] \right\}. \end{aligned} \quad (3.9)$$

Equation 3.9 can be further simplified by recognizing that the expected value in the fourth term can be written in terms of the characteristic function of \vec{r}_i . The characteristic function for a random process \vec{u} is given as

$$\underline{M}_{\vec{u}}(\vec{\omega}) = E[e^{j\vec{\omega} \cdot \vec{u}}], \quad (3.10)$$

where $\vec{\omega}$ is a vector of the same dimension as \vec{u} (4). The characteristic function can also be written in terms of an inverse Fourier transform operation. If \vec{u} is of dimension n , we can write the characteristic function as

$$\underline{M}_{\vec{u}}(\vec{\omega}) = (2\pi)^2 F_n^{-1}[p_n(2\pi\vec{u})], \quad (3.11)$$

where $p_u(\vec{u})$ is the probability density function (pdf) of \vec{u} and F_n^{-1} is the n-dimensional inverse Fourier transform operator. The Fourier transform operators are defined as:

$$F_n[p_u(\vec{u})] = \int p_u(\vec{u}) e^{(-j2\pi\vec{u}\cdot\vec{\omega})} d^n \vec{u} \quad (3.12)$$

$$F_n^{-1}[p_u(\vec{u})] = \int p_u(\vec{u}) e^{(j2\pi\vec{u}\cdot\vec{\omega})} d^n \vec{u} \quad (3.13)$$

Using the results given in equations 3.12 and 3.13 the expected value in the fourth term of eqn 3.9 can be written as

$$E \left[\exp \left\{ j \frac{4\pi}{\lambda} [(\hat{r}_1 - \hat{r}_2) \cdot (\vec{r}_i - \vec{r}_{i'})] \right\} \right] = F_n[F_n^{-1}[p_{i|i'}^r(\vec{r}_i | \vec{r}_{i'})]_{\vec{\omega}=\frac{2}{\lambda}\vec{\Delta}_r} p_{i'}^r(\vec{r}_{i'})]_{\vec{\omega}=\frac{2}{\lambda}\vec{\Delta}_r}, \quad (3.14)$$

where $p_i^r(\vec{r})$ is the pdf of \vec{r}_i , $p_{i|i'}^r(\vec{r}_i | \vec{r}_{i'})$ is the conditional pdf of \vec{r}_i given $\vec{r}_{i'}$. The directional change in the observation point ($\vec{\Delta}_r$) is defined by $\vec{\Delta}_r \doteq \hat{r}_1 - \hat{r}_2$. Using the above results eqn 3.9 can be rewritten as

$$\begin{aligned} R_\sigma(\vec{\Delta}_r) &= NE[| \underline{b}_i |^4] + N^2\alpha^4 - 2N\alpha^4 \\ &+ \alpha^4 \sum_{i=1}^N \sum_{i'=1}^N F_n[F_n^{-1}[p_{i|i'}^r(\vec{r}_i | \vec{r}_{i'})] p_{i'}^r(\vec{r}_{i'})]_{\vec{\omega}=\frac{2}{\lambda}\vec{\Delta}_r}. \end{aligned} \quad (3.15)$$

Assuming the real and imaginary of \underline{b}_i are Gaussian implies that the $| \underline{b}_i |$ is Rayleigh distributed, which is consistent with an earlier assumption concerning the signal pdf given in chapter 2. The first term in eqn 3.15 can be shown to be

$$E[| \underline{b}_i |^4] = 2\alpha^4. \quad (3.16)$$

Using this assumption, eqn 3.15 can now be written as

$$R_\sigma(\vec{\Delta}_r) = N^2\alpha^4 + \alpha^4 \sum_{i=1}^N \sum_{i'=1}^N F_n[F_n^{-1}[p_{i|i'}^r(\vec{r}_i | \vec{r}_{i'})] p_{i'}^r(\vec{r}_{i'})]_{\vec{\omega}=\frac{2}{\lambda}\vec{\Delta}_r} \quad (3.17)$$

If the position of the i th scatterer is independent of the position of the i' scatterer, then eqn 3.17 is given as

$$\begin{aligned} R_{\sigma}(\vec{\Delta}_r) &= N^2\alpha^4 + \alpha^4 \sum_{i=1}^N \sum_{i'=1}^N [F_n^{-1}[p_i^r(\hat{r}_i)]|_{\vec{\omega}=\frac{2}{\lambda}\vec{\Delta}_r} \cdot [F_n[p_{i'}^r(\hat{r}_{i'})]]|_{\vec{\omega}=\frac{2}{\lambda}\vec{\Delta}_r} \\ &= N^2\alpha^4 + \alpha^4 \left| \sum_{i=1}^N F_n^{-1}[p_i^r(\hat{r}_i)]|_{\vec{\omega}=\frac{2}{\lambda}\vec{\Delta}_r} \right|^2. \end{aligned} \quad (3.18)$$

The autocovariance is determined by subtracting the mean squared value of σ from the autocorrelation function (4). Thus, the autocovariance can be written as:

$$K_{\sigma}(\vec{\Delta}_r) = \alpha^4 \left| \sum_{i=1}^N F_n^{-1}[p_i^r(\hat{r}_i)]|_{\vec{\omega}=\frac{2}{\lambda}\vec{\Delta}_r} \right|^2. \quad (3.19)$$

This general model allows us to calculate the signal autocovariance for any given scattering center distribution, $p_i^r(\hat{r})$. The autocovariance is then used to determine P_D using the radar detection model of chapter 2. The next step is to calculate the signal autocovariance for a given distribution of scattering centers. The first distribution considered is where the individual scatterers have a Gaussian distribution about a collection of fixed points in the xy plane. This distribution is chosen since the location and magnitude of the scattering centers can be easily determined from a two dimensional radar image of the target. The second distribution considered is a uniform distribution of scattering centers in a rectangular area of the xy plane. The rectangular scattering center distribution is chosen since the only knowledge required for the calculation of the autocovariance function are the x and y dimensions of the target.

3.1.3 Point Source Scattering Centers The first autocorrelation function we will generate using the above model is for a collection of scattering centers where each scattering center has a Gaussian distribution about a fixed location in the xy plane. This distribution is chosen since it requires the most information about the

target's RCS. Specifically, we require the position and magnitude of each scattering center. The pdf of the position of each scatterer is described by:

$$p_i^r(x, y) = \frac{1}{2\pi\sigma_x\sigma_y} \exp \left\{ \frac{-1}{2} \left[\left(\frac{x - x_i}{\sigma_x} \right)^2 + \left(\frac{y - y_i}{\sigma_y} \right)^2 \right] \right\} \quad (3.20)$$

where σ_x and σ_y are the standard deviations of the i th scattering center about the means x_i and y_i . The inverse Fourier transform of eqn 3.20 is given by

$$\begin{aligned} F_2^{-1}[p_i^r(x, y)] &= \frac{1}{2\pi\sigma_x\sigma_y} \iint \exp \left\{ \frac{-1}{2} \left[\left(\frac{x - x_i}{\sigma_x} \right)^2 + \left(\frac{y - y_i}{\sigma_y} \right)^2 \right] \right\} \\ &\quad \times \exp(j2\pi(x\omega_x + y\omega_y)) dx dy \end{aligned} \quad (3.21)$$

where ω_x and ω_y are the x and y directed components of $\vec{\omega}$. Carrying out the integration of eqn 3.21 gives

$$F_2^{-1}[p_i^r(x_i, y_i)] = \frac{1}{\pi} \exp \left\{ -\frac{\omega_x^2 \sigma_x^2 + \omega_y^2 \sigma_y^2}{2} \right\} \exp \{ j2\pi [(\omega_x x_i + \omega_y y_i)] \}. \quad (3.22)$$

Substituting eqn 3.21 into eqn 3.18 gives

$$R_\sigma(\vec{\Delta}_r) = N^2 \alpha^4 + \left| \sum_{i=1}^N \frac{\alpha_i^2}{\pi} \exp \left\{ -\frac{2\Delta_x^2 \sigma_x^2 + 2\Delta_y^2 \sigma_y^2}{\lambda^2} \right\} \exp \left\{ \frac{j4\pi}{\lambda} [(\Delta_x x_i + \Delta_y y_i)] \right\} \right|^2 \quad (3.23)$$

Subtracting the mean squared value then gives the autocovariance

$$K_\sigma(\vec{\Delta}_r) = \left| \sum_{i=1}^N \frac{\alpha_i^2}{\pi} \exp \left\{ -\frac{2\Delta_x^2 \sigma_x^2 + 2\Delta_y^2 \sigma_y^2}{\lambda^2} \right\} \exp \left\{ \frac{j4\pi}{\lambda} [\Delta_x x_i + \Delta_y y_i] \right\} \right|^2 \quad (3.24)$$

The signal covariance matrix can be calculated from the autocovariance. P_D is then calculated using the detection model developed in chapter 2. Before we proceed with the P_D calculations, we will also determine the autocovariance function for a uniform distribution of scattering centers.

3.1.4 Uniform Distribution of Scattering Centers The second scatterer distribution considered is where the N point scatterers are uniformly distributed within a rectangular area of width L_x and length L_y . This distribution was chosen since it requires the least amount of target information. The pdf for this distribution is easily written as

$$p^r(\vec{r}) = \frac{1}{L_x L_y} \text{rect}\left(\frac{x}{L_x}\right) \text{rect}\left(\frac{y}{L_y}\right), \quad (3.25)$$

where

$$\text{rect}(x) = \begin{cases} 1 & |x| < \frac{1}{2} \\ 0 & \text{elsewhere} \end{cases} \quad (3.26)$$

Application of the the two-dimensional Fourier transform and simplifications, results in the following autocorrelation function

$$R_\sigma(\vec{\Delta}_r) = N^2 \alpha^4 \left[1 + \left\{ \text{sinc}\left(\frac{2L_x \Delta_x}{\lambda}\right) \text{sinc}\left(\frac{2L_y \Delta_y}{\lambda}\right) \right\}^2 \right], \quad (3.27)$$

where the $\text{sinc}(u) = \sin(u\pi)/u\pi$. The corresponding autocovariance function is given by:

$$K_\sigma(\vec{\Delta}_r) = N^2 \alpha^4 \left\{ \text{sinc}\left(\frac{2L_x \Delta_x}{\lambda}\right) \text{sinc}\left(\frac{2L_y \Delta_y}{\lambda}\right) \right\}^2 \quad (3.28)$$

The point source and uniform distribution models gives us two methods of determining the signal autocovariance. The point source distribution requires the most information about the target and is therefore more difficult to implement than the uniform distribution of scatterers. However, the point source distribution will give an accurate prediction of the autocovariance. The uniform distribution is chosen because only the maximum dimension of the target are required and the autocovariance is therefore easily calculated. Finally, we are interested in comparing the predicted autocovariance, $K_\sigma(\vec{\Delta}_r)$ to an empirically derived autocovariance, $\hat{K}_\sigma(k)$. The two covariance prediction models can then be compared to the empirical estimate to see how different target shapes affect the autocovariance.

3.2 Empirical Estimate of the Autocorrelation Function

An empirical estimate of the signal autocovariance function can be obtained from the measured RCS data. This method is useful if the target RCS pattern is known. The empirical results will then be compared to the autocovariance predictions previously developed. The following empirical estimate of the autocorrelation function is given by Levanon(15) and Crispin (3)

$$\hat{R}_\sigma[k] = \frac{1}{N-k} \sum_{k=0}^{N-1-k} z_k^* z_{n+k}, \quad 0 \leq k \leq N-1, \quad (3.29)$$

where z_k is a sequence of target RCS values (m^2). The estimate of the expected value of z is

$$\bar{z} = \frac{1}{N} \sum_{k=0}^{N-1} z_k, \quad (3.30)$$

and the autocovariance estimate is determined by

$$\hat{K}_\sigma = \hat{R}_\sigma[k] - \bar{z}^2. \quad (3.31)$$

3.3 Summary

This chapter has shown how the autocorrelation of the RCS can be predicted for any distribution of scattering centers. The autocovariance was determined for two types of distributions. The uniform distribution is the easiest method to implement since it only requires the maximum dimensions of the target. The point source distribution requires the location and magnitude of the individual scattering centers and is more difficult to implement but should provide a more accurate estimate of the autocorrelation. Finally, we introduced a method for empirically estimating the autocovariance using the measured RCS data. The next chapter compares these two prediction techniques to the empirical estimate of the autocorrelation for a particular complex target.

IV. *Target Model*

In chapter 2 we showed the importance of the correlation parameters in determining P_D of a target. In chapter 3 we developed a technique to describe the signal correlation properties based on the target's scattering center distributions. We also introduced an empirical method of estimating the autocovariance using measured RCS data. Our goal is to model the autocovariance of the target without having to revert to the detailed angular sampling of two samples per RCS lobe. With this goal in mind, the next step is investigate how well the autocovariance prediction techniques estimate the autocovariance of the target.

This chapter illustrates how to use the uniform and point source scattering center distribution predictions to calculate the autocovariance of a complex target. The autocovariance is also empirically estimated from the measured RCS data. This estimate is then compared to the two predicted autocovariances discussed in chapter 3. This comparison is made using the RCS from the AIM-9 missile.

4.1 *AIM-9 Missile*

An AIM-9 missile model is used to show how the autocovariance varies with changes in the observation angle. The 1/3.72 scale model is shown in Figure 4.1. The model was measured at Ohio State University's compact radar range at 36 GHz. The target was measured at a zero degree elevation angle, and in azimuth at every 0.15 degrees from 0 to 180 degrees. The missile was chosen because the spatial extent of the scattering centers are large in the side-on dimension (95 wavelengths), and small in the nose-on dimension (11 wavelengths). The significance of the spatial extent will be shown later. The missile was also chosen since it is a relatively complex target.

The 0 to 180 degrees azimuth RCS plot of the missile at zero degrees elevation is given in Figure 4.2. Note that zero degrees corresponds to the nose-on observation angle, and 90 degrees is the side-on observation angle. As seen from the plot, the

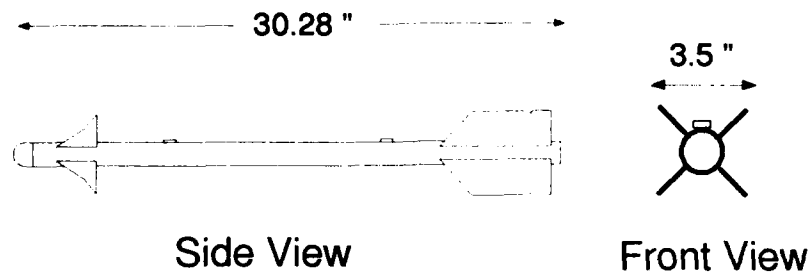


Figure 4.1. AIM-9 Missile

widest lobe width occurs at the nose on aspect angles. The lobes widths become increasingly narrow as the observation angle approaches broadside. The RCS pattern of the target can be more easily seen if the azimuth scale is expanded. A 30 to 60 degrees azimuth plot of the missile is shown in Figure 4.3. Before we proceed further,

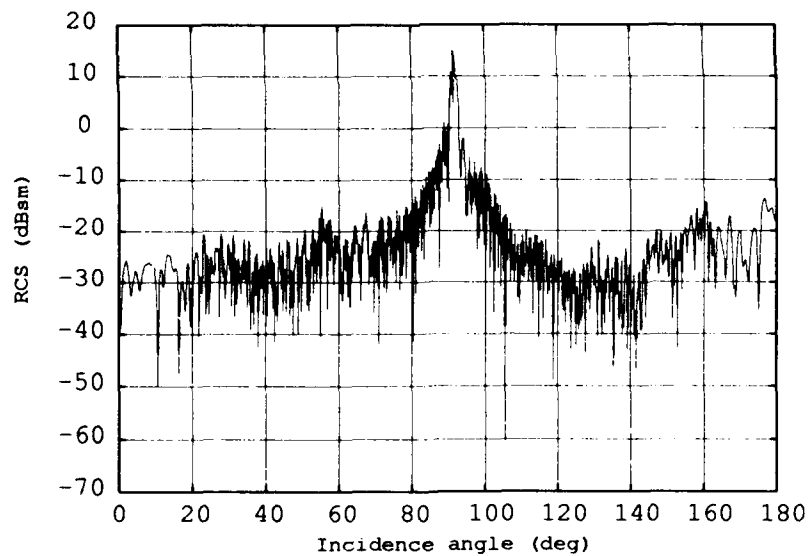


Figure 4.2. 36 GHz, 0° – 180° Missile RCS Azimuth Plot

a brief discussion on the RCS lobing structure will help explain the autocovariance plots shown at the end of this chapter.

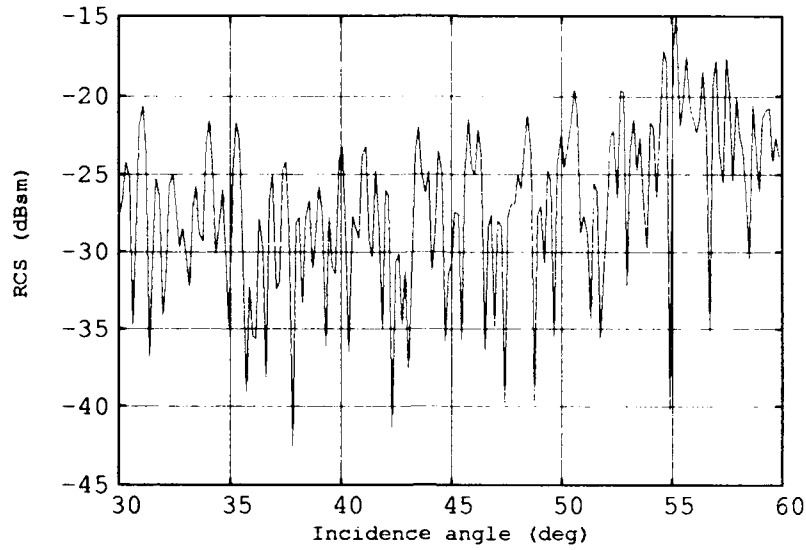


Figure 4.3. 36 GHz, 30° – 60° Missile RCS Azimuth Plot

The RCS lobes widths of a complex target can be estimated from our earlier results of chapter 3. Recall the results of chapter 3 showed the target RCS is given as

$$\sigma(\hat{r}) = \left| \sum_{i=1}^N \underline{b}_i \exp \left\{ j \frac{4\pi}{\lambda} (\hat{r} \cdot \vec{r}_i) \right\} \right|^2, \quad (4.1)$$

where \underline{b}_i is the scalar backscattered field from the i th point scatterer for a unit amplitude incident field and \hat{r} is a unit vector pointing in the direction of the observation point. Using the target/observer geometry of Figure 4.4, eqn 4.1 can be written as

$$\sigma(\theta) = \left| \sum_{i=1}^N \underline{b}_i \exp \left\{ j \frac{4\pi}{\lambda} (x_i \cos \theta + y_i \sin \theta) \right\} \right|^2, \quad (4.2)$$

where θ is the observation angle and is measured from the x -axis and x_i and y_i are the x and y -directed components of \vec{r}_i .

The RCS lobe widths can now be explained by examining eqn 4.2. For small changes in the observation angle, $\Delta\theta$, about $\theta = 0^\circ$, the $\cos(\Delta\theta)$ term is approximately equal to one; however, the $\sin(\Delta\theta)$ term is approximately equal to $\Delta\theta$. As

θ varies by a small amount, the $x_i \cos \theta$ components do not change very quickly compared to the $y_i \sin \theta$ components. The RCS fluctuations are due to the coherent addition of the scattered field for each of the N scattering centers. If $\Delta\theta$ is small, the effects of the scatterers in the x -dimension will be small, and the RCS fluctuations will be determined by the scatterers in the y -dimension. Thus, the RCS lobe widths are determined by the y_i terms in eqn 4.2. At a 90 degree observation angle the cosine terms in eqn 4.2 fluctuate more rapidly than the sine terms and the x_i terms determine the RCS lobe widths.

These results explain the RCS lobing structure of the missile in Figure 4.2. For the 0 degree observation angle, the y -dimension of the scatterers is less than 3.5 inches. As θ is varied, the coherent addition of the scattered field changes slowly, since the y -dimension of the scatterers is small. At a 90 observation angle, the x -dimension of the scatterers is 30.28 inches, almost 10 times larger than the y -dimension, and the resultant RCS lobe widths are about 10 times smaller than the 0 degree observation angle.

4.2 AIM-9 Missile Autocovariance Predictions

The location and relative magnitude of the missile scattering centers were determined from a radar image of the missile. The location of the scattering centers are shown in Figure 4.4 and Table 4.1.

Table 4.1. Locations of the Scattering centers at a 45° Observation Angle

| Scatterer Number | Magnitude (dBsm) | x -Axis Location | y -Axis Location |
|------------------|------------------|--------------------|--------------------|
| 1 | -29.1 | 15.3 in | 0.5 in |
| 2 | -40.5 | 11.1 in | 1.28 in |
| 3 | -41.9 | 10.4 in | 1.71 in |
| 4 | -40.8 | -4.2 in | 0.5 in |
| 5 | -36.8 | -15. in | 0.67 in |

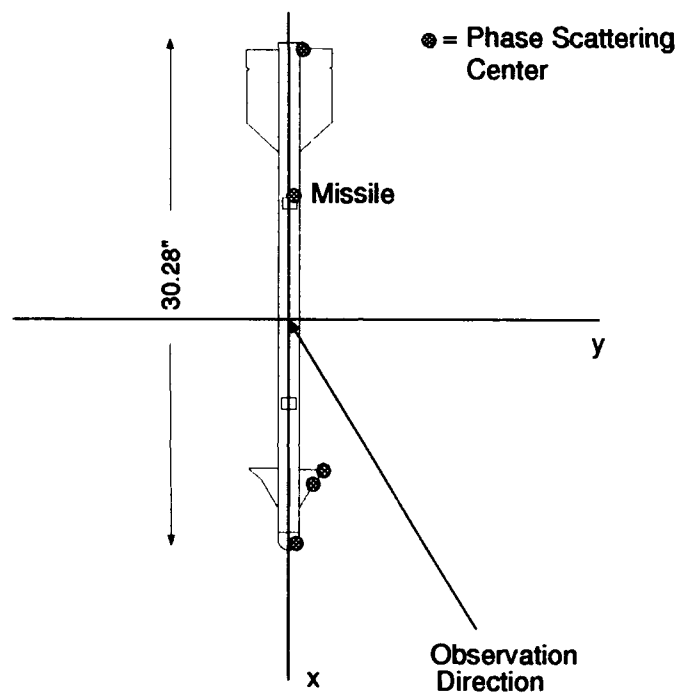


Figure 4.4. Scattering Center Locations at a 45° Observation Angle

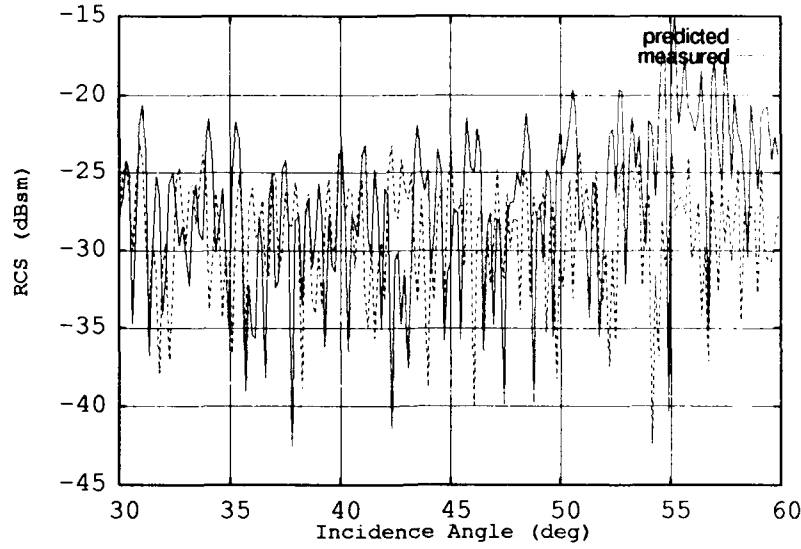


Figure 4.5. Predicted and Measured RCS Azimuth Patterns

The predicted RCS using the point source model was then compared to the measured RCS pattern. The measured RCS and the predicted RCS patterns are shown in Figure 4.5. As seen in the plot, the point source model provides an acceptable approximation to the RCS lobing structure for the missile. The autocovariance function is then determined by eqn 4.3 and the point source scattering locations in Table 4.1. Using eqn 3.24 the autocovariance of the point source distribution is given as

$$K_{\sigma}(\vec{\Delta}_r) = \left| \sum_{i=1}^N \frac{\alpha_i^2}{\pi} \exp \left\{ -\frac{2\Delta_x^2 \sigma_x^2 + 2\Delta_y^2 \sigma_y^2}{\lambda^2} \right\} \exp \left\{ \frac{j4\pi}{\lambda} [\Delta_x x_i + \Delta_y y_i] \right\} \right|^2. \quad (4.3)$$

where $N = 5$ and the locations x_i and y_i correspond to the values in Table 4.1.

The second scattering model is the uniform distribution of scattering centers. Recall from chapter 3 that the autocovariance for this distribution function is given by:

$$K_{\sigma}(\vec{\Delta}_r) = N^2 \alpha^4 \left\{ \text{sinc} \left(\frac{2L_x \Delta_x}{\lambda} \right) \text{sinc} \left(\frac{2L_y \Delta_y}{\lambda} \right) \right\}^2 \quad (4.4)$$

The missile target dimensions L_x and L_y are given as 30.28 inches and 3.5 inches respectively.

4.3 Autocovariance of the AIM-9 Missile at 30, 40, and 45 degrees

The RCS autocovariance is also empirically estimated using the measured RCS data and eqn's 3.29 to 3.31. The autocovariance is calculated for three different observation directions. We will define the de-correlation angle to be the width of the first or main lobe in autocovariance plots. Recall that the de-correlation of the received signal is determined by the RCS lobing structure of the target, i.e. narrower RCS lobes correspond to smaller de-correlation angles. The predicted autocovariance results are shown in figures 4.6 to 4.8.

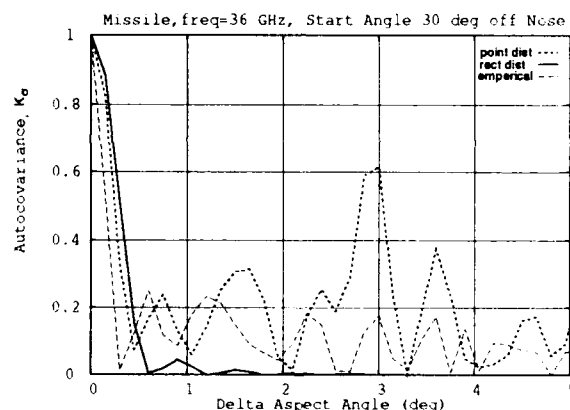


Figure 4.6. Signal Autocovariance, 30 deg off Nose, 5 Scatters

As can be seen from the autocovariance plots the point source distribution and the uniform distribution predictions agree fairly well for all three observation angles. For each of the three cases the point source prediction provides a slightly smaller de-correlation angle than the uniform distribution. For the 30 degree observation angle, the autocovariance based on the measured data provides a smaller de-correlation angle than either the point source or uniform distribution prediction. Recall that the point source locations were determined by a radar image of the target at a 45

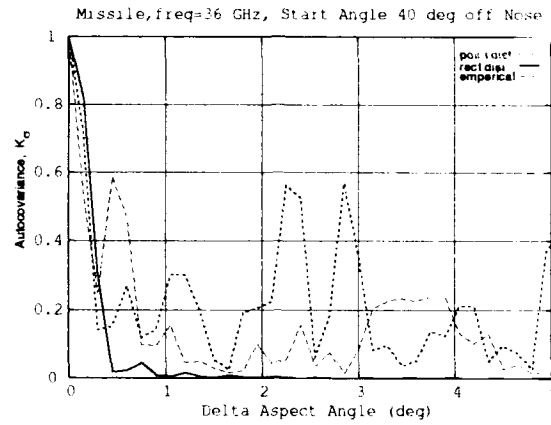


Figure 4.7. Signal Autocovariance, 40 deg off Nose

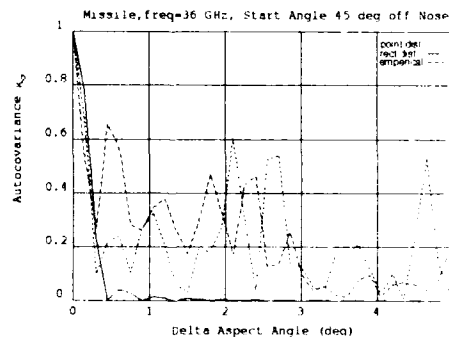


Figure 4.8. Signal Autocovariance, 45 deg off Nose

degree observation angle. As shown in Figure 4.8, the two predicted autocovariances and the empirical estimate give the same de-correlation angle of 0.5 degrees.

4.4 Autocovariance of the AIM-9 Missile at 0, 10, and 30 degrees

The autocovariance was also calculated for the nose-on observation angles. For the point source distribution prediction, the scattering center locations are shown in Table 4.2. For this case, the scattering center locations were also determined from a radar image of the target. The autocovariance was determine for observation directions of 0, 10, and 30 degrees off the nose of the missile. The resultant autocovariance plots are shown in Figure 4.9, 4.10, and 4.11.

Table 4.2. Locations of the Scattering centers at a 0° Observation Angle

| Scatterer Number | Magnitude (dBsm) | <i>x</i> -Axis Location | <i>y</i> -Axis Location |
|------------------|------------------|-------------------------|-------------------------|
| 1 | -40.8 | 15.3 in | 0 in |
| 2 | -39.8 | 10.4 in | 1.17 in |
| 3 | -46.2 | 2.8 in | .5 in |
| 4 | -38.0 | -5.2 in | 0.5 in |
| 5 | -46.8 | -11.6 in | 0.5 in |
| 6 | -52.2 | -8.0 in | 0.5 in |
| 7 | -35.1 | -14.5 in | .67 in |
| 8 | -39.6 | -13.3 in | 1.89 in |
| 9 | -39.8 | 10.4 in | -1.71 in |
| 10 | -46.2 | 2.8 in | -.5 in |
| 11 | -38.0 | -5.2 in | 0.5 in |
| 12 | -46.8 | -11.6 in | -.5 in |
| 13 | -52.2 | -8.0 in | -.67 in |
| 14 | -35.1 | -14.5 in | -1.89 in |
| 15 | -39.6 | -13.3 in | -1.89 in |

For all of the cases considered, the widest de-correlation angle is for the 0 degree observation angle. Figure 4.9 shows the autocovariance for this case. The de-correlation angle is approximately 2.5 degrees. The nose-on autocovariance should have the widest de-correlation angle, since the cross range extent of the target is only

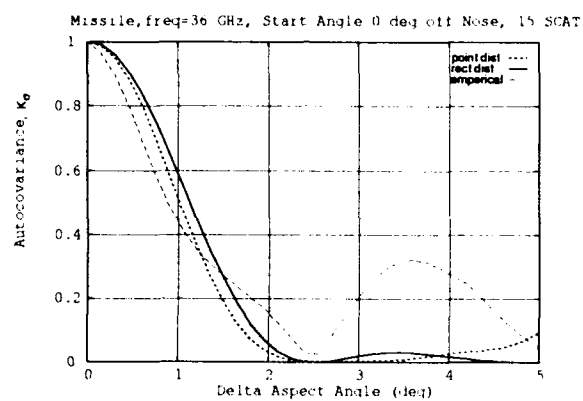


Figure 4.9. Signal Autocovariance, 0 deg off Nose

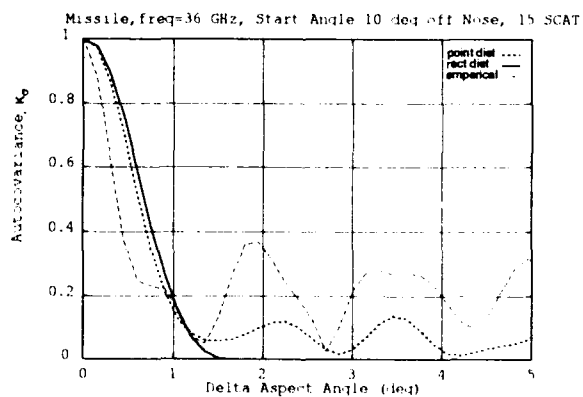


Figure 4.10. Signal Autocovariance, 10 deg off Nose

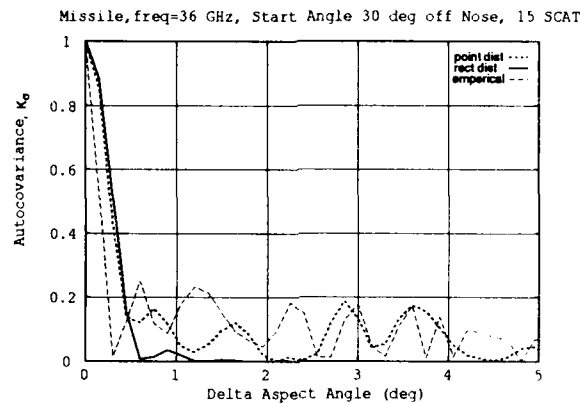


Figure 4.11. Signal Autocovariance, 30 deg off Nose, 15 Scatters

3.5 inches. Remember that the RCS lobe widths are inversely proportional to the cross range extent of the target. Since 0 degrees is the smallest cross range extent, the RCS lobes will be wider and the received signal will fluctuate slower about this observation angle.

For the 0 degree observation angle all three prediction methods provide the same de-correlation angle. Figures 4.9 to 4.11 also illustrate how the de-correlation angle decreases as the observation angle changes from 0 degrees to 30 degrees. For each of the three cases, the point source distribution prediction and the uniform distribution prediction yield approximately the same de-correlation angle, and the empirical estimate yields a slightly smaller de-correlation angle for the 10 degree and 30 degree observation angle cases.

It is also interesting to compare Figure 4.6 to Figure 4.11. For Figure 4.6 the point source locations shown in Table 4.1 were used. The point source locations for Figure 4.11 are from Table 4.2. As shown in the two tables, the distributions differ considerably, 5 scattering centers vs 15 scattering centers; however, the autocovariance plot are approximately the same. Using this observation, it seems reasonable to conclude that a precise determination of the scattering centers is not required to predict the autocovariance properties.

4.5 *Summary*

This chapter has shown how the correlation prediction techniques of chapter 3 are used to determine the autocovariance function for a complex target. For the cases considered, we found the uniform distribution yields approximately the same de-correlation angle as the point source distribution. For other types of targets this might not be the case. The empirical estimate of the autocovariance yields smaller de-correlation angles than the two predictions. In addition, the uniform distribution provides approximately the same de-correlation angle as the point source distribution. Recall that the point source prediction requires the location and relative magnitude of the target scattering centers. Determining the location and magnitude of the scattering centers of a complex target is not easy. The uniform distribution requires only the maximum dimensions of the target and the autocovariance is easily calculated for this type of distribution.

V. Concluding Examples

We are now ready to show how the P_D detection model of chapter 2 and the autocorrelation prediction models of chapters 3 and 4 can be combined to determine P_D for a given radar/target engagement. The results of this chapter will again emphasize the importance of the correlation parameter, ρ , in determining P_D .

We begin this example by defining the target/radar geometry. Once the flight geometry is defined, the correlation parameter ρ is determined from the target autocovariance predictions of chapter 4. P_D is then calculated from the eigenvalues of the signal covariance matrix, using the saddlepoint integration method of chapter 2.

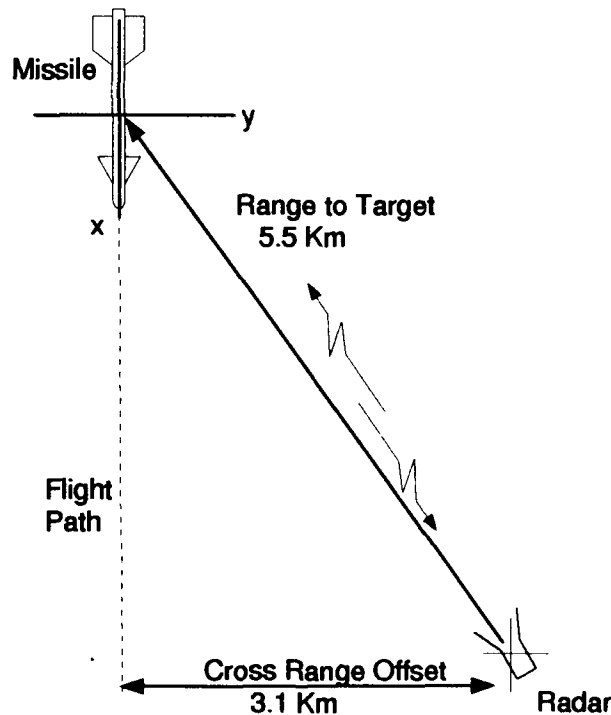


Figure 5.1. Missile/Radar Engagement Geometry

The target/radar engagement geometry is shown in Figure 5.1. The missile's initial position is at 4.5 km down range and 3.1 km cross range from the radar. The velocity of the missile is set at 600 mph (268 m/s), and the missile flies pass the radar maintaining the 3.1 km cross range offset. The missile and radar are at the same altitude, and the pulse repetition frequency of the radar is chosen to be 40 Hz. The probability of false alarm, P_{FA} , is given as 10^{-6} .

For this example, three arbitrary integration intervals were used to illustrate how to calculate P_D using the prediction techniques of chapter 2. The first interval is one second, or 40 integrated pulses. The second interval is 3 seconds (120 pulses), and the third interval is 3.75 seconds (140 pulses). For each of the three cases the initial geometry is shown in Figure 5.1. For this geometry, the initial radar observation angle is 30 degrees off the nose of the missile.

For the 1 second integration interval, the observation angle changes from 30 degrees to 36.7 degrees, as the missile flies pass the radar. The final observation angles for the 3 sec and 3.75 sec integration intervals are 40.5 and 42.1 degrees respectively. Figure 5.2 shows the RCS azimuth plot of the missile for a 30 to 60 degree observation angle.

The autocovariance was calculated using the point source distribution for the scattering center locations given in Table 4.1, and the uniform rectangular distribution model described in chapter 4. The resultant autocovariance functions are shown in Figure 5.3.

Recall that Kanter (14) assumes a single parameter ρ to describe the pulse-to-pulse correlation. This assumption allows the signal autocovariance matrix eigenvalues to be computed in a convenient manner. The criteria for choosing this correlation parameter is somewhat arbitrary. For this analysis, the correlation parameter is defined in the following manner. Referring to figure 5.3, it is easy to see that the autocorrelation approaches zero between 0.5 and 1.0 degrees. The de-correlation angle is defined to be the angle where the autocovariance equals 0.05. To illustrate

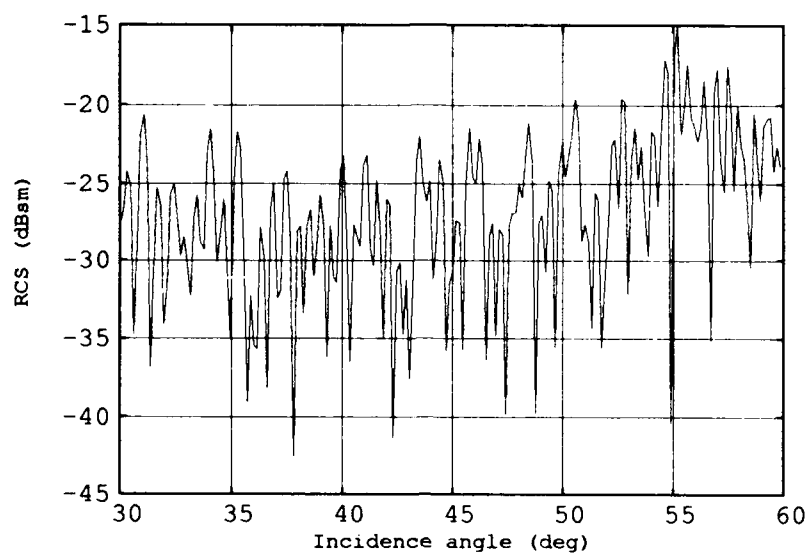


Figure 5.2. Missile RCS Azimuth Plot

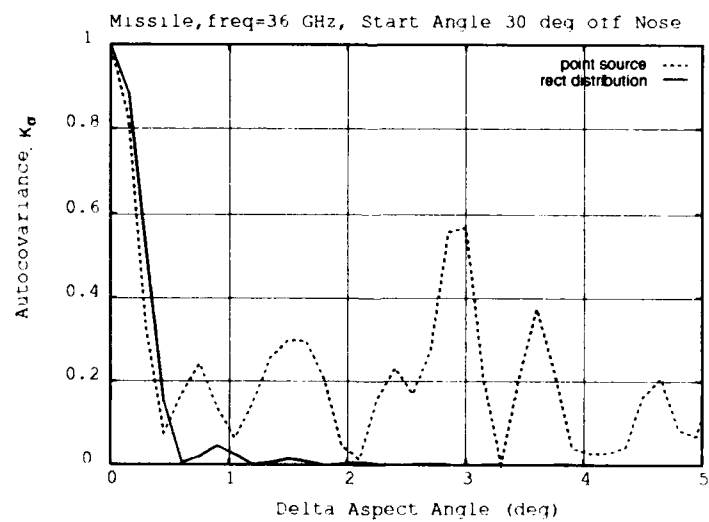


Figure 5.3. Autocovariance for 30 Degrees off Nose

the sensitivity of P_D to the correlation parameter, two additional de-correlation angles of 0.75 and 1.0 degrees were chosen. The pulse-to-pulse exponential correlation parameter, ρ , is determined from the de-correlation angle by

$$\rho = 0.05 \frac{1}{t_\theta \text{prf}}, \quad (5.1)$$

where t_θ is the time for the target to rotate through the de-correlation angle, and prf is the pulse repetition frequency of the radar. Using the above method and the missile/radar engagement geometry described earlier, the de-correlation angles of 0.5, 0.75, and 1.0 degrees correspond to pulse-to-pulse exponential correlation parameters of 0.78, 0.84, and 0.88 respectively. Using these correlation parameters, P_D is calculated for each of the three integration intervals. These results are shown in Figures 5.4, 5.5, and 5.6.

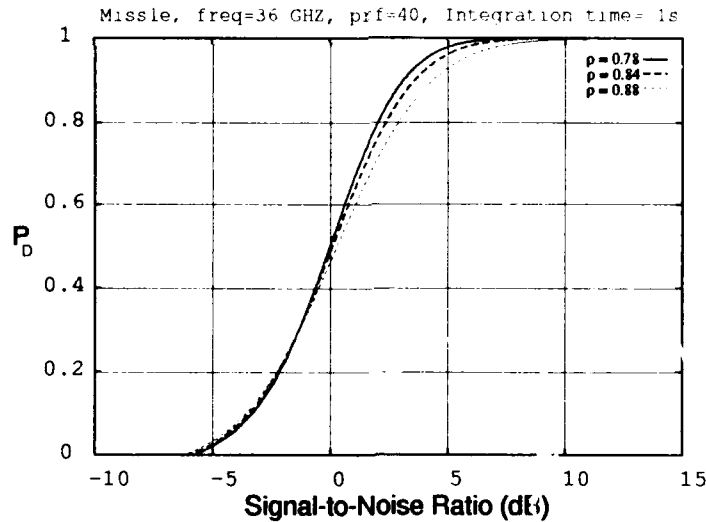


Figure 5.4. P_d for 1 sec Observation Time

Again, for we see the same type of results that we saw in chapter 2. Recall that the more rapidly fluctuating targets have a smaller correlation parameter. For P_D less than 0.4, the correlation parameter has only a marginal effect on the determination of

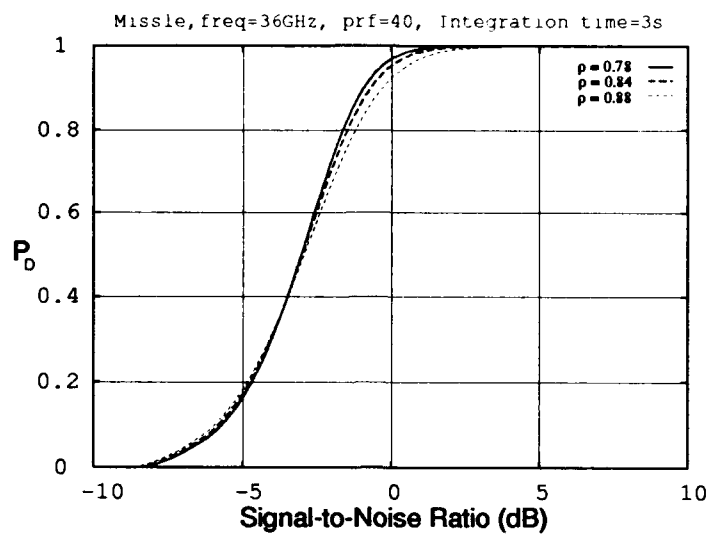


Figure 5.5. P_d for 3 sec Observation Time

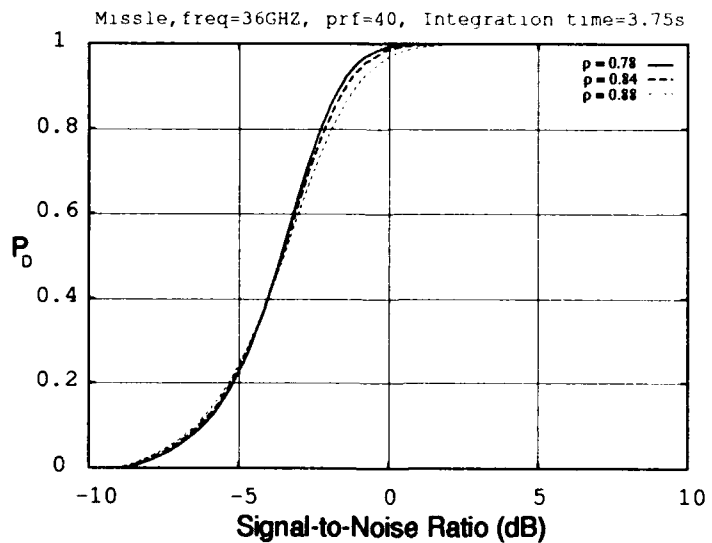


Figure 5.6. P_d for 3.75 sec Observation Time

P_D . For values of P_D greater than 0.4, the correlation parameter becomes important in determining P_D .

Consider the 1 sec integration interval case and $P_D = 0.95$. The less fluctuating signal, $\rho = 0.88$, requires and 1.5 dB higher signal-to-noise ratio to achieve the same P_D as the more fluctuating signal of $\rho = 0.78$. Figures 5.5 and 5.6 also show that the less fluctuating signals required higher signal-to-noise ratios to achieve the same P_D .

The above example illustrates how the detection and correlation models from chapters 2 and 3 can be used to determined the P_D for a given target/radar engagement. This example also illustrates the importance of modeling the correlation properties in determining P_D .

VI. Conclusions

In chapter 2 we showed how the detection of correlated radar returns could be computed. The correlated radar return detection was provided by Swerling (18); however, the required signal covariance eigenvalues are not easily calculated. Kanter (14) provided a convenient means for determining these eigenvalues using an exponential correlation parameter; however, summation errors limited the number of integrated pulses to less than 30. This limitation was overcome through the use of saddlepoint integration and the associated saddlepoint approximations introduced by Carl Helstrom (10). The importance of the correlation parameter ρ in determining P_D was then shown using these techniques.

Chapter 3 provided us with several methods for predicting the signal autocovariance function. The autocovariance is determined by the inverse Fourier transform of the target scattering center distribution. The two distributions we concentrated on were a point source and a uniform distribution; however, other types of distributions could also be used. In addition, we showed how the autocovariance could be empirically estimated from the measured RCS data.

The autocovariance was then predicted for an AIM-9 missile using the techniques described in chapter 3. For this target, the point source and uniform distributions yielded the same de-correlation angle for all the aspect angles considered. Finally, P_D was calculated for the missile using the detection techniques of chapter 2. The results of these calculations once again illustrates the importance of the correlation parameter in determining P_D .

6.1 Follow-on Efforts

The first follow-on effort to this thesis should be to use the detection and correlation prediction techniques to determine the angular RCS sampling requirements.

Additionally, the partially correlation detection techniques could be used to determine how the shape of the autocovariance function affects P_D .

The autocovariance prediction techniques should be applied to other types of targets, to determine if the point source and uniform distributions are the best distributions for predicting the autocovariance.

Appendix A. *Derivation of $L(s)$*

The derivation for the calculating the Laplace transform of $G(v)$ closely follows the original work of Peter Swerling (18). This derivation is included because it provides us with a method for calculating the P_D of partially correlated radar return signals. The radar receiver model and assumptions on the signal statistics are given in chapter 2. Recall that before we can calculate P_D , we first manipulate $G(v)$ into a form which can be integrated. To do this, we first take the Laplace transform, $L(s)$, of the integrated output pdf $G(v)$, which is given as

$$L(s) = \int_0^\infty e^{-sv} G(v) dv. \quad (\text{A.1})$$

The in-phase and quadrature channel detector outputs, x_i and y_i , are defined by the random vectors U^x and U^y as

$$U_x \doteq (x_1, \dots, x_N) \quad U_y \doteq (y_1, \dots, y_N). \quad (\text{A.2})$$

We will also assume that U_x and U_y are mutually statistically independent. U_x and U_y will have identical signal covariance matrixes, C , with individual elements $c_{i,j}$:

$$c_{i,j} = E[z_i z_j], \quad i = 1 \cdots N, \quad j = 1 \cdots N, \quad (\text{A.3})$$

where $E[\cdot]$ is the expectation operator. In-addition, the detector output for the i th pulse is assumed to have a Rayleigh pdf described by

$$p(z_i) = \frac{1}{\bar{z}} \exp\left(-\frac{z_i}{\bar{z}}\right). \quad (\text{A.4})$$

The Laplace transform of $G(v)$ can be computed by first considering the conditional pdf for v . The Laplace transform of this conditional pdf is given by the well known

transform (18)

$$L(s | v) = \frac{1}{(1+s)^N} \prod_{i=1}^N \exp \left[\frac{-s}{1+s} (x_i^2 + y_i^2) \right]. \quad (\text{A.5})$$

The Laplace transform of $G(v)$, $L(s)$, is equal to this expression averaged over the probability distributions of U_x and U_y . Using the mutual independence of the random vectors U_x, U_y , the Laplace transform can be written as

$$L(s) = \frac{1}{(1+s)^N} \int \int \exp \left[- \sum_{i=1}^N \frac{s}{1+s} (x_i^2 + y_i^2) \right] dP(U_x) dP(U_y) \quad (\text{A.6})$$

$$dP(U_x) dP(U_y) = \frac{1}{(2\pi)^N |C|} \exp \left[- \frac{1}{2} \sum_{i,j=1}^N C^{-1} (x_i x_j + y_i y_j) dU_x dU_y \right]. \quad (\text{A.7})$$

Rewriting eqn A.6 with Λ gives $L(s)$ as

$$L(s) = \frac{1}{(1+s)^N} \Lambda, \quad (\text{A.8})$$

where

$$\begin{aligned} \Lambda = & \frac{1}{(2\pi)^N |C|} \int \int \exp \left[- \frac{1}{2} \sum_{i,j=1}^N C^{-1} (x_i x_j + y_i y_j) \right. \\ & \left. - \sum_{i=1}^N \frac{s}{1+s} (x_i^2 + y_i^2) \right] dU_x dU_y \end{aligned} \quad (\text{A.9})$$

Equation A.8 can be further simplified if we define the matrixes $\Psi(s)$ and $\Gamma(s)$ by

$$\Psi(s) \doteq \begin{cases} C^{-1}, & i \neq j \\ C^{-1} + \frac{2s}{1+s}, & i = j \end{cases}, \quad (\text{A.10})$$

and

$$\Gamma(s) \doteq | \Psi(s) |. \quad (\text{A.11})$$

Substituting in the above results, eqn A.9 is reduces to

$$\Lambda = \left[\frac{\Gamma(0)}{\Gamma(s)} \right] \left(\frac{\Gamma(s)}{(2\pi)^N} \int \int \exp \left[-\frac{1}{2} \sum_{i,j=1}^N \Psi(s)(x_i x_j + y_i y_j) \right] dU_x dU_y \right). \quad (\text{A.12})$$

The term in the parenthesis of eqn A.12 is just the integral of the pdf, which equals one. Thus, $L(s)$ reduces to

$$L(s) = \frac{1}{(1+s)^N} \left[\frac{\Gamma(0)}{\Gamma(s)} \right]. \quad (\text{A.13})$$

Equation A.13 can also be expressed in terms of the eigenvalues of $\Psi(s)$ and the eigenvalues of the inverse signal covariance matrix, λ'_i , where

$$\lambda'_i(s) = \lambda'_i + \frac{2s}{1+s}, \quad (\text{A.14})$$

and

$$\Gamma(0) = \prod_{i=1}^N \lambda'_i \quad (\text{A.15})$$

$$\Gamma(s) = \prod_{i=1}^N \left(\lambda'_i + \frac{2s}{1+s} \right). \quad (\text{A.16})$$

Substituting in the above results gives the simplified form of $L(s)$:

$$L(s) = \frac{1}{(1+s)^N} \prod_{i=1}^N \left[1 + \frac{2s}{(1+s)\lambda'_i} \right]^{-1} \quad (\text{A.17})$$

Equation A.17 can also be expressed in terms of the normalized signal covariance matrix eigenvalues if the following substitution is made for λ'_i :

$$\lambda'_i \doteq \frac{2}{\chi \lambda_i}. \quad (\text{A.18})$$

After some minor simplifications, eqn A.17 is given as:

$$L(s) = \prod_{i=1}^N \frac{1}{1 + s(1 + \chi \lambda_i)} \quad (\text{A.19})$$

The P_D is then determined by taking the inverse Laplace transform of eqn A.19 and integrating the resultant pdf from the threshold, V_T to infinity.

Appendix B. *Determination of the Exponential Covariance Matrix Eigenvalues*

The following method of calculating the eigenvalues for an exponential covariance matrix is taken from Irving Kanter's (14) paper on the detection of the correlated radar returns. It is included, because it provides an effective method from calculating the eigenvalues of large matrixes.

First consider the general case where the correlation of noncontiguous pulses may not be neglected. Recall that the eigenvalues of the full C matrix are required to calculate the P_D . The earlier results of chapter 2 neglected the noncontiguous pulses, which made the corresponding signal covariance matrix tridiagonal. The solution of the matrix equation was simplified through the use of the tridiagonal matrix. The same approach for determining the matrix eigenvalues can be used if the signal matrix can be made tridiagonal. This is easily done by noting that the inverse of the signal covariance matrix, C^{-1} , is a tridiagonal matrix. This inverse matrix can be written as

$$C^{-1} = \frac{1}{1 - \rho^2} \begin{bmatrix} 1 & -\rho & 0 & \cdots & 0 \\ -\rho & 1 + \rho^2 & -\rho & 0 & \vdots \\ 0 & \ddots & \ddots & \ddots & 0 \\ \vdots & \ddots & \ddots & 1 + \rho^2 & -\rho \\ 0 & \cdots & 0 & -\rho & 1 \end{bmatrix}. \quad (\text{B.1})$$

The original matrix equation to be solved is

$$[C - \lambda I]U = 0 \quad (\text{B.2})$$

which can be rewritten for the tridiagonal inverse matrix as

$$(1 - \rho^2) \left(C^{-1} - \frac{1}{\lambda} I \right) V = 0 \quad (\text{B.3})$$

Recall the sum of the eigenvalues equals the trace of C giving the relation

$$\sum_{n=1}^N \lambda_n = N. \quad (\text{B.4})$$

The equivalent homogeneous boundary value problem can be written as a set of homogeneous second order difference equations

$$-\rho v_{n-1} + \left(1 + \rho^2 - \frac{1 - \rho^2}{\lambda} \right) v_n - \rho v_{n+1} = 0, \quad n = 1, \dots, N \quad (\text{B.5})$$

with the boundary conditions

$$\begin{aligned} v_0 - \rho v_1 &= 0 \\ v_{N+1} - \rho v_N &= 0 \end{aligned} \quad (\text{B.6})$$

Since the equation is linear and has constant coefficients, there are two solution in the form of

$$v_n = \gamma^n \quad (\text{B.7})$$

where γ is given as

$$\gamma = 1 + \rho^2 - \frac{1 - \rho^2}{\lambda} \pm \frac{\sqrt{\left(1 + \rho^2 - \frac{1 - \rho^2}{\lambda} \right)^2 - 4\rho^2}}{2\rho} \quad (\text{B.8})$$

The condition

$$| (1 + \rho^2 - (1 - \rho^2)/\lambda)/(2\rho) | \geq 1 \quad (\text{B.9})$$

implies either $\lambda \geq (1 + \rho)/(1 - \rho)$ or $\lambda \leq (1 - \rho)/(1 + \rho)$ eqn B.4 cannot be satisfied. Thus, we introduce the real angle θ by

$$\cos \theta \doteq \frac{1 + \rho^2 - \frac{1 - \rho^2}{\lambda}}{2\rho}, \quad (\text{B.10})$$

and write the solution in the form of eqn 2.24. Application of the boundary conditions then yields the equations

$$[1 - \rho \cos \theta]K_1 - [\rho \sin \theta]K_2 = 0 \quad (\text{B.11})$$

$$[\cos(N + 1)\theta - \rho \cos N\theta]K_1 + [\sin(N + 1)\theta - \rho \sin N\theta]K_2 = 0 \quad (\text{B.12})$$

whose determinant must vanish. Thus, θ obeys the transcendental equation

$$\sin(N + 1)\theta - 2\rho \sin N\theta + \rho^2 \sin(N - 1)\theta = 0. \quad (\text{B.13})$$

Since the values $\theta = 0, \pi$ do not permit a nontrivial solution to the boundary value problem, the roots of eqn B.13 again lie in the open interval $(0, \pi)$. Since it has not been possible to solve eqn B.13 analytically, the following remarks allow a numerical solution to be easily achieved: To show that there are exactly N roots between 0 and π , we first write as

$$[(1 + \rho^2) \cos \theta - 2\rho] \sin N\theta + [(1 - \rho^2) \sin \theta] \cos N\theta = 0 \quad (\text{B.14})$$

and then introduce the function $\phi(\theta)$ by means of

$$\sin \phi(\theta) \doteq \frac{(1 - \rho^2) \sin \theta}{1 + \rho^2 - 2\rho \cos \theta} \quad (\text{B.15})$$

$$\cos \phi(\theta) \doteq \frac{(1 + \rho^2) \cos \theta - 2\rho}{1 + \rho^2 - 2\rho \cos \theta} \quad (\text{B.16})$$

so that eqn B.14 becomes

$$\sin[N\theta + \phi(\theta)] = 0. \quad (\text{B.17})$$

The derivative of ϕ with respect to θ yields the condition:

$$\frac{d\phi}{d\theta} = \frac{1 - \rho^2}{1 + \rho^2 - 2\rho \cos \theta} > 0 \quad (\text{B.18})$$

$\phi(\pi)$ can then be expressed as:

$$\phi(\pi) = \phi(0) + \int_0^\pi \frac{1 - \rho^2}{1 + \rho^2 - 2\rho \cos \theta} d\theta = \pi \quad (\text{B.19})$$

Equation B.17 represents a modulated sinusoid whose total phase increases monotonically from 0 at $\theta = 0$ to $(N + 1)\pi$ at $\theta = \pi$, it has exactly N distinct zero crossings in the open interval $(0, \pi)$.

Further, since $d^2\phi/d\theta^2 < 0$ in $(0, \pi)$ and $d\phi/d\theta = 1$ at $\cos \theta = \rho$, the function $\sin[N\theta + \phi(\theta)]$ oscillates more rapidly than does $\sin(N + 1)\theta$ in the domain $0 < \theta < \cos^{-1} \rho$ and more slowly (but still more rapidly than does $\sin(N\theta)$ in the domain $\cos^{-1} \rho < \theta < \pi$. Using these observations concerning the spacing of the roots, it is an easy matter to accurately locate the roots by means of a Newton-Raphson method.

Denoting the roots by $\theta_1, \dots, \theta_N$ the eigenvalues are given by

$$\frac{1 - \rho}{1 + \rho} < \lambda_n = \frac{1 - \rho^2}{1 + \rho^2 - 2\rho \cos \theta_n} < \frac{1 + \rho}{1 - \rho} \quad (\text{B.20})$$

Note that the expansion of eqn B.20 into a power series in ρ yields a first order approximation which is identical to eqn 2.27.

Bibliography

1. Barton, D.K. and H.R. Ward. *Handbook of Radar Measurement*, chapter 6, 163-182. Artec House, Inc, 1984.
2. Blake, Lamont V. *Radar Range-Performance Analysis*, chapter 1, 100-200. Artec House, Inc, 1986.
3. Crispin, J.W. and K.M. Siegel. *Methods of Radar Cross-Section Analysis*. Academic Press, 1968.
4. Davenport, Wilbur B. Jr. *Probability and Random Processes*. McGraw-Hill Book Co., 1987.
5. DiFranco, J.V. and W. L. Rubin. *Radar Detection*, chapter 11, 373-445. Artec House, Inc, 1980.
6. DiFranco, J.V. and W. L. Rubin. *Radar Detection*, chapter 10, 364-371. Artec House, Inc, 1980.
7. Edrington, T. S. "The Amplitude Statistics of Aircraft Radar Echoes," *IEEE Transactions on Military Electronics*, 9:10-16 (January 1965).
8. Haykin, Simon S. *Detection and Estimation, Application to Radar*, chapter 1, 0-300. Dowden, Hutchinson, and Ross, Inc., 1976.
9. Helstrom, C. W. and J. A. Ritcey. "Evaluating radar detection probabilities by steepest descent integration," *IEEE Transactions on Aerospace and Electronic Systems*, AES(20):624-634 (September 1984).
10. Helstrom, Carl W. "Approximate evaluation of detection probabilities in radar and optical communications," *IEEE Transactions on Aerospace and Electronic Systems*, AES(14):630-640 (July 1978).
11. Helstrom, Carl W. "Evaluating the detectability of Gaussian stochastic signals by steepest descent integration," *IEEE Transactions on Aerospace and Electronic Systems*, AES(19):428-437 (May 1983).
12. Helstrom, Carl W. "Detection Probabilities for Correlated Rayleigh Fading Signals," *IEEE Transactions on Aerospace and Electronic Systems*, 28(1):259-267 (January 1992).
13. IMSL Problem-Solving Software Systems. "User's Manual Math/Library FORTRAN Subroutines for Mathematical Applications,". Houston, Texas, 1987.
14. Kanter, Irving. "Exact Detection Probability for Partially Correlated Rayleigh Targets," *IEEE Transaction on Aerospace and Electronic Systems*, 22(2):184-195 (March 1986).

15. Levanon, Nadav. *Radar Principles*, chapter 2, 0-300. John Wiley and Sons, Inc., 1988.
16. Schwartz, Mischa. "Effects of Signal Fluctuation on the Detection of Pulse Signals in Noise," *IRE Transactions on Information Theory*, 66-71 (June 1956).
17. Skolnik, Merrill I. *Introduction to Radar Systems*. New York: McGraw-Hill Book Company, 1980.
18. Swerling, Peter. "Detection of Fluctuating Pulsed Signals in the Presence of Noise," *IRE Transaction on Information Theory*, 175-178 (September 1957).
19. Swerling, Peter. "Probability of Detection for Fluctuating Targets," *IRE Transaction on Information Theory*, IT(6):273-308 (April 1960).
20. Welsh Byron, Joseph Phillip and Pyati Vittal. "RCS Autocovariance Functions and Power Spectral Densities of Complex Targets." Unpublished report, Air Force Institute of Technology, 1991.

Vita

Alan L. Buterbaugh was born on 4 June 1959 in Warren, Ohio. In 1977, he graduated from Southeast High School and enlisted in the United States Air Force. While enlisted, he served as an Avionics Sensor Systems Technician for the Tactical Air Command. In 1985, he received a Bachelor of Science in Electrical Engineering from The University of Akron. After receiving his commission at The University of Akron in 1985, he was assigned to the Aeronautical Systems Division, Wright-Patterson AFB, where he worked as a Low Observables engineer for the B-2 Special Program Office. He was selected in January 1991 to attend the School of Engineering, Air Force Institute of Technology.

Permanent address: 7947 Newton Falls Rd
Ravenna, OH 44266

REPORT DOCUMENTATION PAGE

Form Approved
OMB No. 0704-0188

Public reporting burden for this collection of information is estimated to average 1 hour per response, including the time for reviewing instructions, searching existing data sources, gathering and maintaining the data needed, and completing and reviewing the collection of information. Send comments regarding this burden estimate or any other aspect of this collection of information, including suggestions for reducing this burden, to Washington Headquarters Services, Directorate for Information Operations and Reports, 1215 Jefferson Davis Highway, Suite 1204, Arlington, VA 22202-4302, and to the Office of Management and Budget, Paperwork Reduction Project (0704-0188), Washington, DC 20503.

| | | | | |
|--|--|---|--|--|
| 1. AGENCY USE ONLY (Leave blank) | | 2. REPORT DATE September 1992 | 3. REPORT TYPE AND DATES COVERED Master's Thesis | |
| 4. TITLE AND SUBTITLE The Detection and Correlation Modeling of Rayleigh Distributed Radar Signals | | | 5. FUNDING NUMBERS | |
| 6. AUTHOR(S) Alan L. Buterbaugh | | | | |
| 7. PERFORMING ORGANIZATION NAME(S) AND ADDRESS(ES) Air Force Institute of Technology, WPAFB OH 45433-6583 | | | 8. PERFORMING ORGANIZATION REPORT NUMBER AFIT/GE/ENG/92S-03 | |
| 9. SPONSORING, MONITORING AGENCY NAME(S) AND ADDRESS(ES) Capt Pete Collins 6585 Test Group Radar Scatterer Div Holloman AFB NM 88330-5000 | | | 10. SPONSORING, MONITORING AGENCY REPORT NUMBER | |
| 11. SUPPLEMENTARY NOTES | | | | |
| 12a. DISTRIBUTION / AVAILABILITY STATEMENT Distribution Unlimited | | | 12b. DISTRIBUTION CODE | |
| 13. ABSTRACT (Maximum 200 words) <p style="text-align: center;">Abstract</p> <p>This thesis provides a method for determining the detection of partially correlated Rayleigh distributed radar returns by a pulsed search radar. The receiver consists of a quadrature demodulator receiver, followed by a square law envelope detector and a linear post-detection integrator. In addition, a technique for determining the pulse-to-pulse correlation of a complex target is given using inverse Fourier transforms of the target scattering centers. An AIM-9 missile is used to illustrate how the partially correlated detection techniques and the pulse-to-pulse correlation predictions can be used to determine the probability of detection.</p> | | | | |
| 14. SUBJECT TERMS The Detection and Correlation Modeling of Rayleigh Distributed Radar Signals | | | 15. NUMBER OF PAGES 78 | |
| | | | 16. PRICE CODE | |
| 17. SECURITY CLASSIFICATION OF REPORT UNCLASSIFIED | 18. SECURITY CLASSIFICATION OF THIS PAGE UNCLASSIFIED | 19. SECURITY CLASSIFICATION OF ABSTRACT UNCLASSIFIED | 20. LIMITATION OF ABSTRACT UL | |